BRL R 1757

BRL

REPORT NO. 1757

EFFECT OF EXTERNAL THERMAL RADIATION ON THE BURNING RATE OF DOUBLE-BASE SOLID PROPELLANTS (STEADY STIMULUS)

M. M. Ibiricu
W. P. Aungst
F. A. Williams

February 1975

USA BALLISTIC RESEARCH LABORATORIES
ABERDEEN PROVING GROUND, MARYLAND

UNCLASSIFIED

SECURITY CLASSIFICATION OF THIS PAGE *(When Data Entered)*

REPORT DOCUMENTATION PAGE		READ INSTRUCTIONS BEFORE COMPLETING FORM
1. REPORT NUMBER REPORT NO. 1757	2. GOVT ACCESSION NO.	3. RECIPIENT'S CATALOG NUMBER
4. TITLE *(and Subtitle)* EFFECT OF EXTERNAL THERMAL RADIATION ON THE BURNING RATE OF DOUBLE-BASE SOLID PROPELLANTS (Steady Stimulus)		5. TYPE OF REPORT & PERIOD COVERED 6. PERFORMING ORG. REPORT NUMBER
7. AUTHOR(s) M. M. Ibiricu W. P. Aungst F. A. Williams (Univ. of California, San Diego)		8. CONTRACT OR GRANT NUMBER(s)
9. PERFORMING ORGANIZATION NAME AND ADDRESS USA Ballistic Research Laboratories Aberdeen Proving Ground, Maryland 21005		10. PROGRAM ELEMENT, PROJECT, TASK AREA & WORK UNIT NUMBERS 1T161102A32C-03
11. CONTROLLING OFFICE NAME AND ADDRESS U.S. Army Materiel Command 5001 Eisenhower Avenue Alexandria, Virginia 22304		12. REPORT DATE FEBRUARY 1975 13. NUMBER OF PAGES 74
14. MONITORING AGENCY NAME & ADDRESS*(if different from Controlling Office)*		15. SECURITY CLASS. *(of this report)* UNCLASSIFIED 15a. DECLASSIFICATION/DOWNGRADING SCHEDULE

16. DISTRIBUTION STATEMENT *(of this Report)*

Approved for public release; distribution unlimited.

17. DISTRIBUTION STATEMENT *(of the abstract entered in Block 20, if different from Report)*

18. SUPPLEMENTARY NOTES

19. KEY WORDS *(Continue on reverse side if necessary and identify by block number)*

Solid Propellant Combustion
Burning Rate Model
Double-Base Propellants
Thermal Radiation Effect
Stabilizer Effect

20. ABSTRACT *(Continue on reverse side if necessary and identify by block number)* jah

A model has been developed that describes the thermal interaction of an externally applied radiant energy flux with the combustion zone of a burning homogeneous solid propellant. It is shown that only the radiation reaching the propellant surface, and absorbed within the solid phase, can effectively induce burning rate augmentation. The burning rate has been found to increase linearly as a function of flux for small radiation intensities and less than linearly as the flux becomes larger. Many conditions have been investigated in detail,

DD FORM 1 JAN 73 1473 EDITION OF 1 NOV 65 IS OBSOLETE

UNCLASSIFIED

SECURITY CLASSIFICATION OF THIS PAGE *(When Data Entered)*

including the limiting cases of solid-phase surface absorption and deep in-depth absorption with heat generation. This extensive examination has permitted the identification of the necessary conditions for treating the effect of radiation as an increase in the initial propellant temperature. The conditions at which such an equivalence principle is not applicable have also been identified. This is a new and significant finding. The effect of thermal radiation is closely related to the propellant parameter known as temperature sensitivity. By extension of the theory, important subsidiary effects on temperature sensitivity have been identified, particularly the role of stabilizers and other propellant ingredients. Experiments verify well the theoretical predictions.

TABLE OF CONTENTS

TABLE OF CONTENTS (Cont'd)

LIST OF ILLUSTRATIONS

NOMENCLATURE

A	Preexponential constant in Arrhenius rate of solid-phase reaction.
B	Preexponential constant in Arrhenius rate of gas-phase reaction.
c	Solid heat capacity per unit mass.
c_p	Gas specific heat at constant pressure.
D	Diffusion coefficient.
E	Activation energy for gas-phase reaction.
E_s	Activation energy for solid-phase reaction.
H	Heat released in solid interior by main decomposition reaction, per unit mass of reactant consumed.
H_l	Heat released in solid interior by stabilizer reaction, per unit mass of reactant consumed.
H_g	Heat released in gas-phase reaction per unit mass of reactant consumed.
K	Parameter defined by Eq (28).
L	Sum of heat of gasification and heat conducted into interior of solid, both per unit mass of solid gasified.
L_s	Heat of gasification per unit mass of solid at temperature T_s.
m	Mass burning rate.
n	Pressure exponent of burning rate.
P	Steady combustion pressure.
Q	External effective radiant energy flux.
Q_1	External radiant energy flux absorbed in-depth by solid.
Q_2	External radiant energy flux absorbed by solid gasification layer.
R	Universal gas constant.
r	Regression rate of solid.
T	Temperature.
T_f	Flame temperature.
T_i	Initial temperature of solid.
T_s	Temperature of solid surface.
t	Time.
x	Distance normal to solid surface.
x_f	Distance between solid surface and gas-phase reaction zone.

NOMENCLATURE (Cont'd)

Y	Reactant mass fraction.
α	Gas diffusivity.
Λ	Burning rate eigenvalue.
λ	Solid thermal conductivity.
λ_g	Gas thermal conductivity.
μ	Absorption coefficient for solid.
ν	Reaction order of gas-phase reaction.
ξ	Nondimensional distance in solid.
Π_T	Temperature sensitivity coefficient of burning rate.
ρ	Solid density.
ρ_g	Gas density.
σ	Nondimensional absorption coefficient for solid.
τ	Nondimensional solid temperature.

Subscript

o	Denotes absence of external radiant energy flux.

I. INTRODUCTION

A new theoretical analysis aimed at developing a better understanding of the influence of thermal effects in solid propellant combustion is given here. It also aims at obtaining burning rate predictions which exhibit explicitly the dependence on radiant flux. Practical motivation ranges from interest in burning rate control to concern about detonation suppression.

Solid propellant burning is sustained by several modes of energy release and transfer. Heat generation in the solid phase and heat feedback from the gas-phase flame to the burning surface are major driving mechanisms, depending upon which process is controlling. The study of thermal effects, derived by stimulating the burning propellant with an external source of radiant energy, constitutes a fundamental method of testing the applicability of combustion models, and has the experimental advantage of readily available equipment. This method also has the theoretical advantage that many important interpretations can be made without having to resort to uncertain descriptions of flame structure or schemes about the intricate chemical reactions taking place. The analysis is based on energy considerations with no direct inclusion of chemistry; i.e., the chemical reactions involved are assumed to proceed faster with added thermal energy but not differently.

Because of the more immediate interest of double-base propellants in Army applications, this type of solid propellant has been investigated first. Composite propellants may be considered later in the study and have not been included here. Therefore, the multiplicity of conditions that characterize the combustion of double-base propellants within rocket operating pressures have been examined in detail. The descriptions of the interaction between the thermal radiation and the combustion zone result from limiting procedures involving the three principal solid-phase lengths of surface reaction, heat conduction, and radiation absorption. By allowing the absorption length to vary over a wide range, the effect of external radiant energy is determined for each condition

of interest. When the absorption length becomes very small, surface gasification appears to dominate and no effect from the external radiation is predicted, provided that the gas-phase flame is not controlling. Generation of heat in the interior of the solid phase can also become an important factor when the radiation is absorbed deep inside the solid.

To simplify the presentation of results, the thermal stimulus provided by the external source is represented by the net extra flux which would be effectively absorbed at the burning propellant surface after allowing for losses along the optical path. This indirectly supposes that the product gases are transparent, which is of course not true. Metallized propellants are excluded from the experiment for this reason, and not because of any theoretical requirement. The surface gasification and gas flame reaction are represented by Arrhenius rate expressions assumed to have a high activation energy. The surface and final flame temperatures are viewed in the traditional sense as free parameters arrived at by energy balance. No assumptions, however, are introduced regarding the temperature profile between the surface and final temperatures or regarding other elements of flame structure.

In the past, the consideration of thermal effects in solid propellant combustion evolved from a very specialized practical problem. It concerned the degree of augmentation of burning rate in rocket chambers as compared to the strand-burner rate.[1*] The augmentation observed for the same pressure was explained in terms of the thermal radiation field generated inside the rocket chamber. From this early work comes the hypothesis of equivalence between heat absorbed and increase in initial propellant temperature. The present study has confirmed the appropriateness of this "equivalence principle", and has extended its validity through a rigorous treatment of the problem. It has further yielded the very important theoretical result of delineating the unique burning conditions under which the equivalence principle fails to apply.

---

*References are listed on page 55.

Another practical aspect of the thermal effect is the temperature sensitivity of solid propellant combustion. As a general problem, the temperature dependence is a primary propellant parameter (likewise the pressure dependence), which cannot be defined without highly accurate combustion models, currently nonexistant. Conceptually, however, this problem is a part of the general theory of thermal effects. The findings of this work are also significant in this regard, by showing the strong effect that solid phase heat generation from individual reactants, like stabilizers, can have on temperature sensitivity.

The main result can be summarized as follows. Somewhere in the overall combustion zone there is a kinetic process which determines the burning rate; the radiation absorbed after this control zone is equivalent to an increase in initial propellant temperature; the radiation absorbed outside is ineffective. The exception to this rule is the case of absorption occurring right at the surface reaction layer accompanied by a change in surface temperature, and provided that the gas-phase flame is not controlling the burning rate. Extremely opaque solid propellants burning at low pressures probably fall in this category. Also, if the external thermal radiation were to cause substantial photochemical changes in the combustion process, a different type of exception would appear. No positive evidence has been found for this phenomenon, however. As for the experimental verification of results, double-base propellants burning in a linear regime at the usual rocket pressures are the logical choice. Nonlinear burning propellants, i.e., propellants exhibiting pronounced mesa or plateau regions, have complicated and unknown pressure and temperature dependences that need to be resolved first by appropriate combustion modelling.

II. GAS-PHASE FLAME REACTION AND SOLID-PHASE RESPONSE

A. Deposition of External Radiation

The analysis is based on the one-dimensional burning of a homogeneous solid propellant. The solid phase occupies the region $x<0$ and the gas-phase the region $x>0$; external radiation is incident

on the propellant from the gas. Because of losses along the optical path, some attenuation of the initial radiation intensity occurs. Losses by gas absorption can be significant, especially in metallized propellants, as well as losses by reflection at the propellant surface. Emission of radiation by the solid will usually be a small correction. In principle the analysis is applicable in the presence of losses; it is only necessary to define the radiant flux, Q, as the one that actually reaches the propellant surface.

Transport of radiation within the solid phase is a truly complicated phenomenon. Deposition of radiation by absorption and scattering are very important for real propellants; however, a detailed optical and mathematical treatment would remain far from practical application. Therefore, both processes are lumped into an empirical Beer's law relationship, $Qe^{\mu x}$, with an effective overall absorption coefficient μ, to be determined experimentally. Scattered radiation leaving the surface is counted as reflection. This assumed law has the right general functional form and thus provides a good practical description of the phenomenom.

Other assumptions pertain to the physical properties. The dependence of μ on the wavelength of the radiation is not simple[2], but it is preferable to use a value of μ corresponding to the wavelength range of most of the radiant flux. There should be no difficulty in doing this unless, for example, half of the radiation is absorbed deep in-depth and the other half at the surface. Anyway, μ is taken to be a known constant. Experimentally determined values of μ range from about 10 cm^{-1} for fairly transparent to almost 200 cm^{-1} for very opaque propellants, 80 to 100 cm^{-1} being more often the average for double-base propellants. For simplicity, the heat capacity, thermal conductivity, and density of the solid are assumed constant. Corresponding assumptions are made for the gas, but these are stated in Appendix A, giving the analysis of the gas-phase reaction zone. The solid phase is considered first, since that is where the radiation makes itself felt initially.

B. Solid-Phase Temperature Profiles

The treatment of the thermal response of the solid phase without in-depth heat generation includes the further assumption that the length of the surface layer, where chemical reaction occurs, is very small compared with either the lengths of the heat conduction zone or the radiation absorption zone. If gasification is a true interface process (e.g., vaporization), then there is no approximation at all. However, although propellants have a polymeric structure, and polymers tend to gasify by in-depth degradation, it has been shown that even in this case, and because of the high activation energy for degradation, the reaction zone length is typically less than one-tenth the length of the heat conduction zone.[3] Except for propellants of unusually high opacity, it is unlikely that the radiation can be absorbed strongly enough for most of it to be deposited in a layer thin compared with the very narrow reaction zone. Therefore, approximating the solid-phase reaction zone as an interface seems justified. Figure 1 illustrates some of the definitions.

The temperature field within the solid, occupying the region $x<0$, is described by the equation

$$\rho c \frac{\partial T}{\partial t} + mc \frac{\partial T}{\partial x} = \lambda \frac{\partial^2 T}{\partial x^2} + \frac{\partial Q}{\partial x} \quad , \tag{1}$$

where T is the temperature, m, the mass burning rate, ρ, the solid density, c, the solid heat capacity per unit mass and λ, the solid thermal conductivity. The symbol Q, already defined, represents the incident external radiant energy flux reaching the solid surface, and having the spatial distribution previously stated,

$$Q(x) = Qe^{\mu x} \quad . \tag{2}$$

In general, Q can be a function of time also, but this part of the study concerns only stimulation under steady-state conditions. Thus,

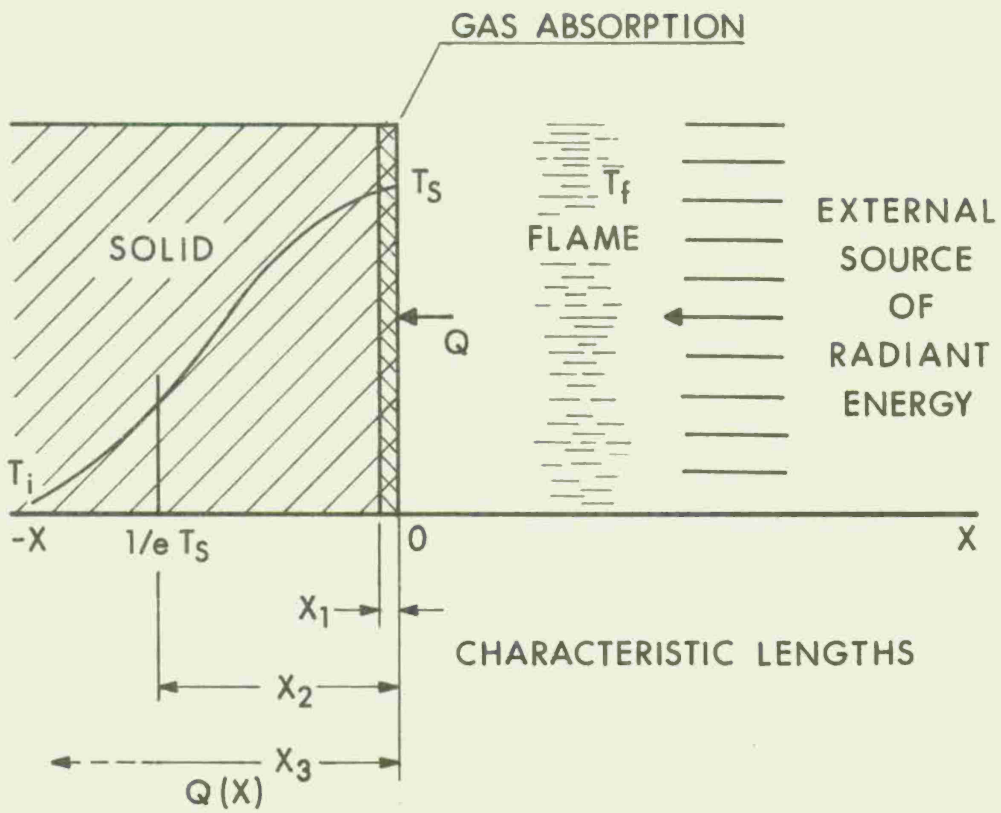

HEAT CONDUCTION $\quad X_2 = \dfrac{\lambda}{r \rho c}$

SURFACE GASIFICATION $\quad X_1 = X_2 \dfrac{RT_S}{E_S}$

RADIATION ABSORPTION $\quad X_3 = \dfrac{1}{\mu}$

Figure 1. Effective Radiant Energy Flux and Characteristic Lengths in Solid.

with Q independent of time, Eq (1) becomes

$$mc \frac{dT}{dx} = \lambda \frac{d^2T}{dx^2} + Q\mu e^{\mu x} \quad . \tag{3}$$

The boundary conditions for Eq (3) are an interface condition involving the flux $\lambda\, dT/dx$ at $x = 0$ and

$$T = T_s \text{ at } x = 0 \ , \tag{4}$$

and

$$T = T_i \text{ at } x = -\infty \ , \tag{5}$$

where T_s is the surface temperature and T_i the initial temperature. An interface energy conservation condition, generally applicable, is

$$\left(\lambda \frac{dT}{dx}\right)_s = m\,(L - L_s) \ , \tag{6}$$

which in this form has the solid-phase pyrolysis process occurring within the interface. In Eq (6), L represents the sum of the heat of gasification and the heat conducted into the interior of the solid, both per unit mass of gasified solid; and L_s represents the heat of gasification at temperature T_s per unit mass of gasified solid.

In nondimensional form, Eq (3) is

$$\frac{d\tau}{d\xi} = \frac{d^2\tau}{d\xi^2} + e^{\sigma\xi} \ , \tag{7}$$

where τ is the nondimensional solid temperature

$$\tau = \frac{(T - T_i)m^2c^2}{Q\mu\lambda} \ , \tag{8a}$$

ξ the nondimensional distance in the solid

$$\xi = \frac{mcx}{\lambda} \ , \tag{8b}$$

and σ the nondimensional absorption coefficient for the solid

$$\sigma = \frac{\mu\lambda}{mc} \ . \tag{8c}$$

The boundary conditions are now

$$\tau = 0 \text{ at } \xi = -\infty \ , \tag{9}$$

and from Eq (6) at $\xi = 0$,

$$\frac{d\tau}{d\xi} = \frac{m^2 c \ (L - L_s)}{Q\mu\lambda} \ . \tag{10}$$

The solution to Eq (7) with the boundary condition of Eq (9) is

$$\tau = Ae^{\xi} + \frac{e^{\sigma\xi}}{\sigma \ (1 - \sigma)} \ . \tag{11}$$

The boundary condition in Eq (10) requires that

$$A = \frac{m^2 c \ (L - L_s)}{Q\mu\lambda} - \frac{1}{1 - \sigma} \ . \tag{12}$$

Therefore, in dimensional form, the solution for T is

$$T = T_i + \left(\frac{L - L_s}{c} \right) e^{\frac{mcx}{\lambda}} + \frac{Q}{mc} \left(\frac{e^{\mu x} - \frac{\mu\lambda}{mc} e^{\frac{mcx}{\lambda}}}{1 - \frac{\mu\lambda}{mc}} \right) . \tag{13}$$

This equation implies, through evaluation at $x = 0$ that

$$T_s = T_i + \frac{L - L_s}{c} + \frac{Q}{mc} \ . \tag{14}$$

Thus, an alternative way to write Eq (13) is

$$T = T_i + (T_s - T_i) e^{\frac{mcx}{\lambda}} + \frac{Q}{mc} \left(\frac{e^{\mu x} - e^{\frac{mcx}{\lambda}}}{1 - \frac{\mu\lambda}{mc}} \right) . \tag{15}$$

Furthermore, the heats of gasification L_s and L_{so}, with and without radiant flux present, respectively, are related by the thermodynamic identity

$$L_s = L_{so} + (c_p - c) \ (T_s - T_{so}) \ , \tag{16}$$

where c_p is the specific heat at constant pressure for the gas and T_s and T_{so} the surface temperature with and without radiant flux present, respectively. Figure 2 illustrates typical examples of radiant energy and temperature distributions in the solid phase.

C. Limiting Cases of Behavior

Eqs (13) and (15) contain two characteristic lengths, the heat conduction length, given by λ/mc, and the radiation absorption length, given by $1/\mu$. As indicated before, both these lengths are assumed large compared with the length of the solid-phase reaction zone. Three limiting cases occur, which cover the alternative situations that could be encountered in practice.

1. Radiation Absorption Length Large Compared with Heat Conduction Length. (i.e., $\mu << mc/\lambda$). In this case there are two distinct regions predicted by Eq (13) or (15). Restricting attention to the position where the heat conduction zone is closest to the surface, the term $e^{\mu x}$ varies here very slowly and is nearly unity. Therefore, Eq (15) can be written as

$$T = \left(T_i + \frac{Q}{mc}\right) + \left[T_s - \left(T_i + \frac{Q}{mc}\right)\right] e^{\frac{mcx}{\lambda}} . \qquad (17)$$

This expression clearly indicates that the only change produced by the radiation is to raise the effective initial temperature to the value

$$T_{i\ eff} = T_i + \frac{Q}{mc} . \qquad (18)$$

At the surface of the solid, the temperature profile in the heat conduction zone, as well as all profiles in hotter regions outside, are the same as they would be if the initial temperature of the propellant were $T_{i\ eff}$.

2. Radiation Absorption Length Small Compared with Heat Conduction Length (i.e., $\mu >> mc/\lambda$). In this case, Eq (13) simplifies to the approximate relation

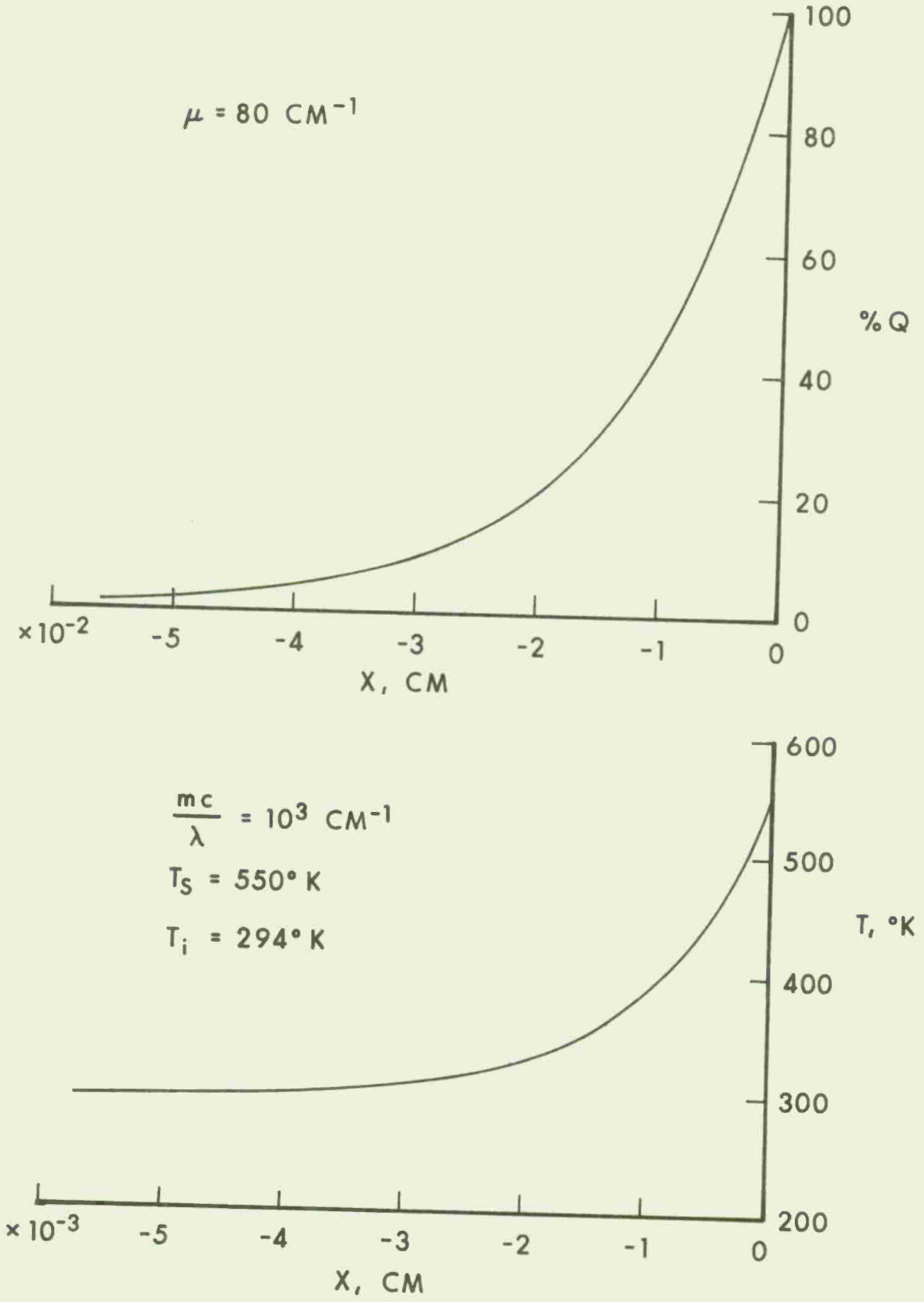

Figure 2. Calculated Distributions of Radiant Energy and Temperature in Solid Phase.

$$T = T_i + \left(\frac{L - L_s}{c} + \frac{Q}{mc}\right) e^{\frac{mcx}{\lambda}} , \qquad (19)$$

at all positions except the very narrow layer at the surface of the solid. The interpretation here is that instead of the gasification requiring an amount of heat L_s at the surface, it now requires a lesser amount, $L_s - (Q/m)$, because of the additional energy input at the surface. The initial propellant temperature remains T_i in Eq (19) and the heat conduction zone maintains its single exponential structure. Effectively, the absorption of radiation merely modifies the energetics at the interface. Therefore, provided the gas-phase reaction is not controlling and the surface temperature adjusts itself, no effect on burning rate will occur.

3. Radiation Absorption Length Equal or Nearly Equal to the Heat Conduction Length (i.e., $\mu = mc/\lambda$ or $\mu \simeq mc/\lambda$). This case separates the two previous limiting cases. When the two lengths are identically the same, ($\mu = mc/\lambda$), the form of the solutions in Eqs (13) and (15) is indeterminate. By solving the problem through limiting procedures, a term involving x exp (mcx/λ) must appear. Since it is unlikely that the two lengths will be exactly equal, the solution for this case is not important. When the two lengths are approximately of the same magnitude, the equations must be used as they stand without further simplification.

D. Applicability of Equivalence Principle

As indicated above, the condition $\mu << mc/\lambda$ allows the effect of external radiant energy input to be equivalent in all respects to an increase in initial temperature by an amount Q/mc, the result given by Eq (18). However, a further condition should be satisfied which concerns the applicability of the steady-state approximation itself. If the propellant is too transparent, then this steady-state effective initial temperature might not be achieved in the course of an experiment. The magnitude of the nonsteady transient is derived from Eq (1). The characteristic time for the solid to respond to deep in-depth radiant absorption can be calculated by balancing the first and last terms

in Eq (1). Since the characteristic temperature rise that needs to be achieved is Q/mc, the balance produces the characteristic time

$$t^* = \frac{\rho c}{m\mu} \quad . \tag{20}$$

This implies that if t^* corresponds to the time the external radiation is applied, then achieving steady-state behavior in the experiment requires that $\mu >> \rho c/mt^*$. Therefore, the general condition for the radiation effect to be equivalent to an increase in initial temperature can be written as

$$\frac{\rho c}{mt^*} << \mu << \frac{mc}{\lambda} \quad . \tag{21}$$

The upper condition on μ given above can be relaxed for many applications. When μ is comparable to mc/λ, the temperature profile in the heat conduction zone of the solid is altered, but the burning rate change is still equivalent to an initial temperature increase, provided that none of the chemical reactions controlling the burning rate occur in this heat conduction zone. In fact, if the chemical reactions of importance occur only in the gas-phase flame, even the surface absorption case, $\mu >> mc/\lambda$, is formally equivalent to an increase in effective initial temperature insofar as the burning rate is concerned. The basic requirement for the burning rate to be described by $T_{i\ eff}$ is that the radiant energy be absorbed beneath the zone in which are occurring whatever chemical reactions that control the burning rate.

Whenever the radiation effect can be viewed as an increase in initial propellant temperature, the situation possesses a great advantage, viz., there is no requirement for a theoretical combustion model capable of predicting the burning rate. The effect of thermal radiation can be obtained even if the structure of the reaction zone is exceedingly complicated. The calculation is done through the coefficient of temperature sensitivity, as discussed in Section IV. Of course, this procedure implies that the dependence of burning rate on initial temperature is known experimentally over the pressure range of interest.

E. Burning Rate Augmentation

The ultimate effect of the radiant flux on the combustion of the propellant is to increase its burning rate, pressure conditions remaining constant. The magnitude of the burning rate augmentation is derived by incorporating the equivalence principle into the rate expressions. Since either the gas-phase or the solid-phase reaction can independently control the burning rate under varying conditions, these two alternative cases are examined separately.

1. Control by Gas-Phase Reaction. The analysis of the gas-phase reaction zone is given in Appendix A. The activation energy is assumed to be high. Under gas-phase control, even the case of radiation absorption at the solid surface satisfies the equivalence rule, and can be described as an effect on initial propellant temperature. The analysis of the gas phase is done in such a way that it can fit quasisteadily into a full time-dependent analysis of the solid phase. The final expression for the gas-phase flame model takes the form

$$m = CP^{\nu/2} e^{-E/2RT_f} , \tag{22}$$

where m is the mass burning rate, C, a constant independent of time, P, the pressure, ν, the order of reaction, E, the activation energy and T_f, the flame temperature. Eq (22) states that for a given reaction order, the burning rate is a unique function of pressure and flame temperature. The radiation will not influence the combustion pressure but it will change the flame temperature through energy conservation. Eq (A8) of Appendix A can be written dimensionally as

$$T_f = T_s + \frac{H_g - L}{c_p} \tag{23}$$

where H_g is the heat released by the gas-phase reaction per unit mass of reactant consumed; other symbols have been previously defined. Combining Eq (23) with Eqs (14) and (16) gives the overall energy conservation condition,

$$T_f = T_{so} + \frac{1}{c_p}\left[H_g - L_{so} - c\,(T_{so} - T_i)\right] + \frac{Q}{mc_p} \,. \tag{24}$$

The zero subscript denotes, as before, the condition with no external radiation present, i.e., a reference condition. Eq (24) is seen to be identical with

$$T_f = T_{fo} + \frac{Q}{mc_p} \,, \tag{25}$$

as expected. Substitution of Eq (25) into Eq (22) yields

$$\frac{m}{m_o} = \exp\left[\frac{E}{2RT_{fo}}\left(\frac{Q}{Q + mc_pT_{fo}}\right)\right]. \tag{26}$$

Eq (26) is the theoretical result for burning rate augmentation, conveniently expressed in terms of the burning rate ratio as a function of the radiant flux Q and other well defined parameters. Most instances of practical interest are likely to have $Q << mc_pT_{fo}$, hence Eq (26) may be well approximated by

$$\frac{m}{m_o} = \exp\left(\frac{KQ}{(m/m_o)}\right) \,, \tag{27}$$

where the coefficient K is defined by

$$K \equiv \frac{E}{2RT_{fo}^2 m_o c_p} \,. \tag{28}$$

The effect predicted by Eq (27) is shown graphically in Figure 3. This plot can be used to verify experimental results whenever the value of K defined by Eq (28) is known.

For small values of the nondimensional parameter KQ, Eq (27) reduces to

$$\frac{m}{m_o} = (1 + KQ) \,, \tag{29}$$

and for very large values of Q, Eq (26) gives the limit

$$\frac{m}{m_o} \to \exp\left(\frac{E}{2RT_{fo}}\right) \text{ as } Q \to \infty \,. \tag{30}$$

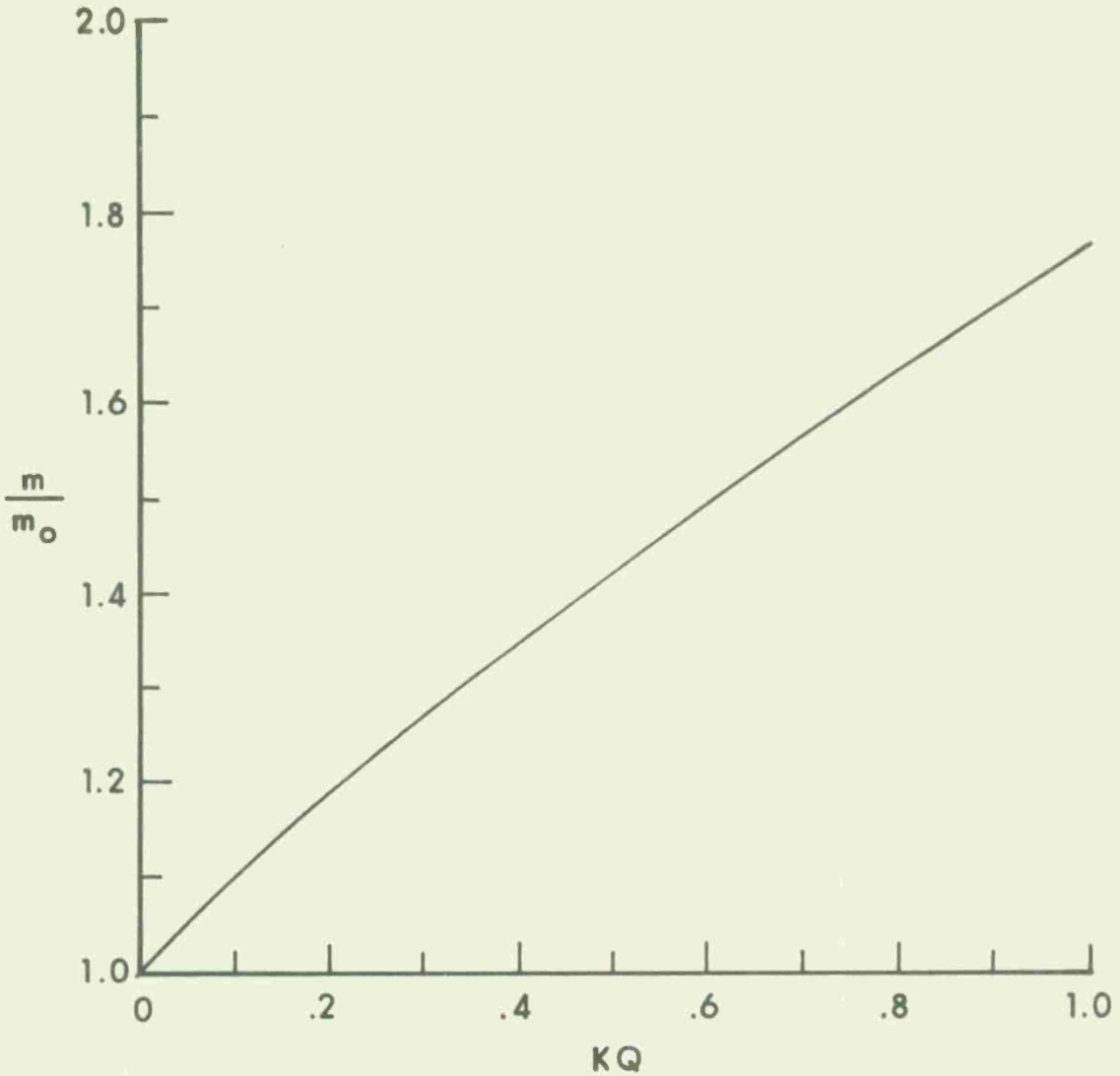

Figure 3. Theoretical Prediction of Burning Rate Augmentation.

Eqs (27) and (29) indicate that for small values of absorbed radiant flux, the augmented burning rate, m, increases roughly linearly with the stimulus, in contrast with the less than linear effect predicted at progressively higher levels of stimulation. At these higher values, the increase in burning rate causes the dependence on radiant flux to be less pronounced. The derivative of Eq (27) is

$$\frac{dm}{dQ} = \frac{m_o K}{1 + \frac{KQm}{m_o}} \tag{31}$$

which for sufficiently small values of the parameter KQ reduces to

$$\frac{dm}{dQ} = m_o K \ . \tag{32}$$

This result is in agreement with the analysis of Coates and Kwak,[4] who obtained reasonable good agreement with experiment for values of K that seem realistic.

2. Control by Solid-Phase Reaction. There are circumstances when the reaction controlling the burning rate occurs in the solid phase rather than in the gas phase. For a number of double-base propellants this is believed to occur, at least in certain pressure ranges. In this case, the previous treatment is equally applicable with suitable modifications. A burning rate expression of the form

$$m = A e^{-E_s/2RT_s} \ , \tag{33}$$

takes the place of Eq (22), A being a constant that involves the preexponential factor, and E_s is the activation energy. The energy feedback from any gas-phase flame is now assumed negligible. Two other conditions are that the radiation must be absorbed in the propellant beyond the surface reaction zone, and that a certain amount of heat must be released by a solid-phase reaction. This problem is extensively investigated in the next Section. Then an adiabatic energy conservation condition determines the surface temperature T_s, and the end result is an expression like Eq (33). Therefore, Eq (27) still holds, but with

the coefficient K now defined as

$$K_s \equiv \frac{E_s}{2RT_{so}^2 m_o c} \quad . \tag{34}$$

The new coefficient K_s is larger than the corresponding coefficient K for the gas phase, mainly because T_{so} is smaller than T_{fo}, so that a stronger burning rate augmentation can be expected from the same external radiant stimulus Q under solid-phase control.

Konev[5] worked out a different theory by assuming that T_s remains T_{so} in the presence of external radiation. This implies the existence of a fixed gasification temperature for the solid surface, which seems doubtful because the temperature adjusts itself to maintain the steady state. Therefore his result is questionable. Of course, his results for the opposite case, deep in-depth absorption of radiation, are not. Konev's later experiments appear to be the most accurate of all and his reported data verify well the predictions for the above case. As seen here, this is the case of greatest interest for practical propellants.

III. SOLID-PHASE REACTION ZONE

A. Inclusion of Heat Generation

Exothermicity within the solid phase may contribute significantly to the burning rate particularly for double-base propellants. Work by collaborators of Konev[6] has employed this view to obtain a simplified description of all aspects of the combustion of double-base propellants, including effects of external radiation. This work, as well as much related work on solid-phase exothermicity, adopts a burning rate formula of Zeldovich[7] which is not exactly correct in the limit of high activation energy. Because of its interest and potential importance, an improved treatment of solid-phase reactions with absorption of radiation is developed here.

For a solid in the region $x<0$, the conservation equations may be written in the form

$$m\frac{dY}{dx} = -w \ , \tag{35}$$

where w is the reaction rate and Y, the mass fraction of reactant in the solid, and

$$mc\frac{dT}{dx} = \lambda \frac{d^2T}{dx^2} + Hw + Q\mu e^{\mu x} \ , \tag{36}$$

where H is the heat released in the solid-phase reaction per unit mass of reactant consumed, other than by activity of the propellant stabilizers. The remaining symbols have the same meaning as in Section II. Reactant diffusion within the solid is neglected, and for simplicity, a zero-order reaction is assumed, allowing the reaction rate w to take the form

$$w = \rho A e^{-E_s/RT} \ , \tag{37}$$

where A is the preexponential factor in sec^{-1}, and E_s is the activation energy for the solid-phase reaction. The boundary conditions for Eqs (35) and (36) are

$$Y = 0 \quad \text{at} \quad x = 0 \ , \tag{38a}$$

$$T = T_s \ \text{at} \quad x = 0 \ , \tag{38b}$$

and

$$Y \to 1 \quad \text{as} \quad x \to -\infty \ , \tag{39a}$$

$$T = T_i \ \text{as} \quad x \to -\infty \ . \tag{39b}$$

The surface temperature is specified in the traditional manner, through surface heat transfer and other processes to be considered later.

Similarly to the gas-phase analysis, the result seeks the asymptotic solution for large activation energy. There develops a

convective-diffusive zone where the solution to Eq (35) is Y = 1, and Eq (36) reduces to

$$mc\frac{dT}{dx} = \lambda \frac{d^2T}{dx^2} \quad , \tag{40}$$

under the assumption that no radiation is absorbed in the convective-diffusive zone. Only limiting cases of the analysis given in Section II will be used. The solution to Eq (40) is

$$T = T_i + constant\ e^{\frac{mcx}{\lambda}} \quad , \tag{41}$$

and substituting for the simplest case, when Q = 0 and the rate w is localized at the surface, shows that the constant is $(T_s - T_i)$.

There is reason to generalize Eq (41) by assuming that an exothermic reaction, releasing a small amount of heat, occurs within this zone. The reaction is interpreted to be the well known reaction between the stabilizer and the nitroglycerin or nitrocellulose.[1,6] The resulting temperature profile differs from Eq (41) and depends on the rate of the new reaction, whose activation energy is not likely to be as large as E_s. Assuming that the new reaction goes to completion early, only the temperature gradient at the zone-end nearest to the propellant surface is needed. In this region, if the new reaction liberates the heat H_1, then Eq (41) changes via energy conservation to

$$T = T_i + \frac{H_1}{c} + constant\ e^{\frac{mcx}{\lambda}} \quad . \tag{42}$$

Defining

$$T_H = T_i + \frac{H_1}{c} \quad , \tag{43}$$

Eq (42) takes the form

$$T = T_H + (T_s - T_H)\ e^{\frac{mcx}{\lambda}} \quad . \tag{44}$$

The next point to consider is the way in which radiant energy modifies

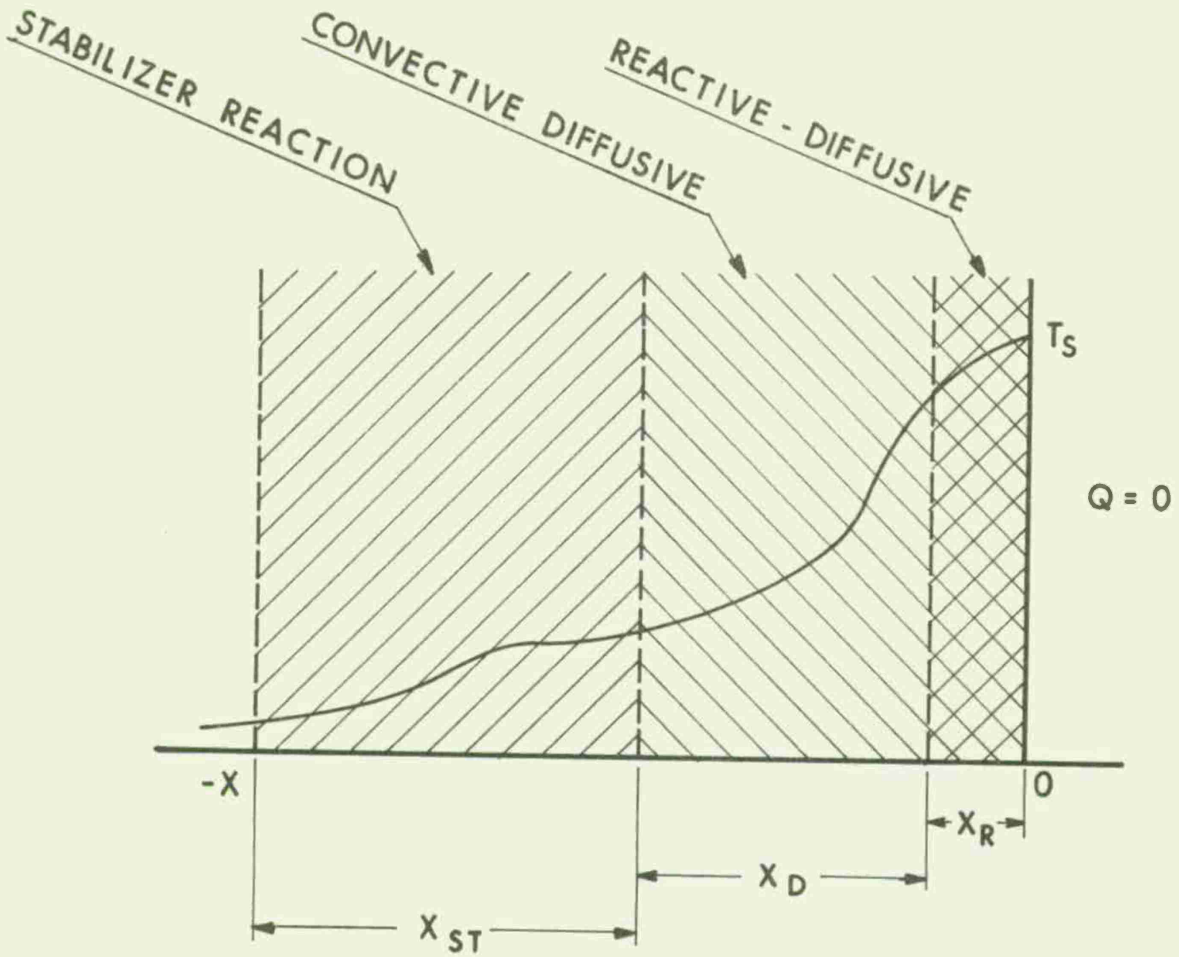

$$X_{ST} \gg X_D \gg X_R$$

Figure 4. Solid-Phase Reaction Zones Without External Radiation.

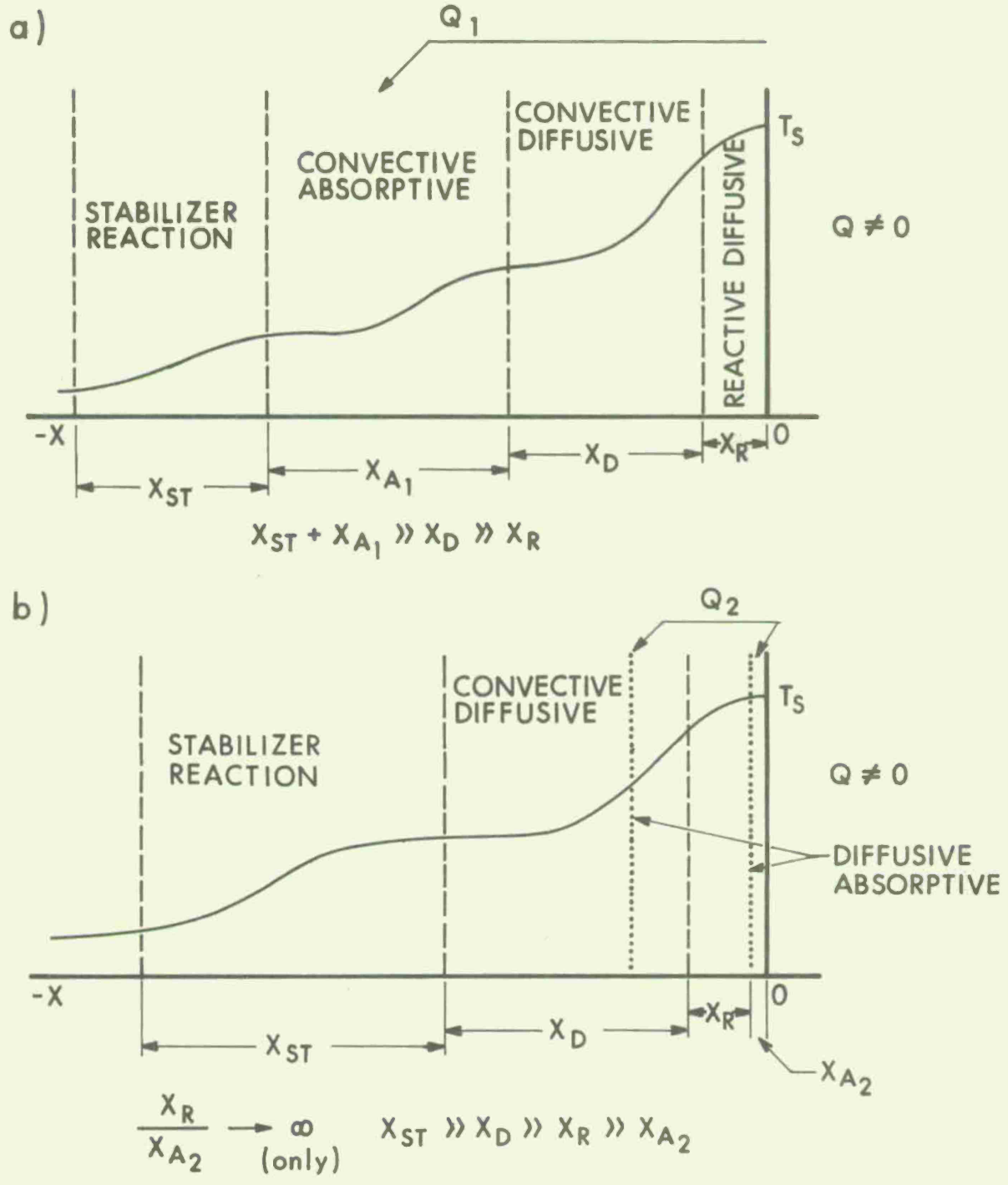

Figure 5. Solid-Phase Reaction Zones With External Radiation.

Eq (44). Figures 4 and 5 qualitatively illustrate the temperature profiles and other definitions of the solid-phase reaction zone.

B. Limiting Cases of Behavior

There are again two final cases of interest. To obtain a general expression capable of exhibiting two limiting types of behavior, the following approach is utilized. It considers that out of the total radiant flux Q reaching the surface, a portion Q_1 is absorbed in the interior of the solid as prescribed by the condition $\mu << mc/\lambda$ and the remainder Q_2, is absorbed as prescribed by the condition $\mu >> mc/\lambda$, under different localized possibilities. It will be later ascertained that the radiation Q_2 needs to be treated in detail only when its absorption takes place in a layer of the same or smaller length than the surface reaction zone.

1. Effect of Radiation Q_1, Having an Absorption Length Large Compared with the Heat Conduction Length. For $\mu << mc/\lambda$, the radiation is absorbed in a convective-absorptive zone deep inside the solid. Its effect then appears in much the same way as H_1. Therefore, Eq (44) is changed to

$$T = T_i + \frac{H_1}{c} + \frac{Q_1}{mc} + \left(T_s - T_i - \frac{H_1}{c} - \frac{Q_1}{mc} \right) e^{\frac{mcx}{\lambda}} , \qquad (45)$$

where the constant of integration has been evaluated by using the requirement of Eq (38b), that $T = T_s$ at $x = 0$, the lowest-order matching result. This case is depicted in Figure 5 (a).

2. Effect of Radiation Q_2, Having an Absorption Length Small Compared with the Heat Conduction Length. For $\mu >> mc/\lambda$, the radiation is absorbed in a diffusive-absorptive zone located adjacent to the convective-diffusive zone, which is illustrated in Figure 5 (b). There are two limiting possibilities depending upon whether the diffusive-absorptive zone length is large of small compared with the length of the

reaction zone, which is located at the solid surface in the limit of high activation energy. If the diffusive-absorptive zone length is large, then the reaction zone solution should be matched to this instead of to the convective-diffusive zone. This case merits no further analysis, since in a sense it is intermediate and is not likely to be encountered in practice. It requires three distinct length scales to coexist simultaneously such that $\lambda/mc >> 1/\mu >> \lambda/\beta mc$, where β is a nondimensional activation energy defined in Appendix B. The remaining significant possibility is when Q_2 is absorbed in a length of the same or smaller size than the reaction zone length. The full analysis is carried out in Appendix B.

C. Burning Rate Relationship

The resulting burning rate expression, derived in Appendix B, for the complete solid-phase reaction zone, takes the following dimensional form

$$m^2 = \frac{RT_s^2 \lambda \rho A e^{-E_s/RT_s}}{E_s \left[c(T_s - T_i) - \frac{H}{2} - H_1 - \frac{Q_1}{m} \right]} . \qquad (46)$$

It may be at first surprising that Q_2 does not appear in Eq (46). However, upon reflection this result is seen to be entirely consistent with the previous finding that for short absorption lengths, the radiant flux is equivalent to a decreased heat of gasification. A total heat balance would exhibit a dependence of m upon Q_2, but with the surface temperature assumed independent of Q_2 the radiation absorbed at the surface zone is ineffective on burning rate. This result differs from the theoretical result of Konev,[5] which contains an explicit relation between m and Q_2. The Konev result comes from an approximate treatment of the reaction zone, not rigorously valid in the limit of high activation energy. In particular, both the surface temperature and the surface temperature gradient are specified in the Konev treatment. The present analysis indicates, (see Appendix B), that the surface temperature

gradient is determined by the steady-state solution, and that at $x = 0$

$$\frac{\lambda}{mc}\left(\frac{dT}{dx}\right)_s = \frac{T_s - T_i}{T_s} - \frac{H + H_1}{cT_s} - \frac{Q_1}{mcT_s} \quad . \tag{47}$$

Essentially, Konev[5] has not considered Eq (35), needed to ascertain the burning rate through analysis of reactant consumption.

D. Generalization of the Zeldovich Formula

It is of interest to compare Eq (46) with the expression that Zeldovich developed in considering the standard case of $H_1 = 0$ and $Q_1 = 0$. Zeldovich equation is[7]

$$m^2 = \frac{2RT_s^2\ \lambda\rho HA\ e^{-E_s/RT_s}}{E_s\left[c\left(T_s - T_i\right)\right]^2} \quad . \tag{48}$$

It is seen that the RHS of Eq (46) must be multiplied by the term

$$\frac{H\left[2c(T_s - T_i) - H\right]}{\left[c(T_s - T_i)\right]^2} \quad , \tag{49}$$

to recover the Zeldovich equation for the standard case. To recover the generalization of the Zeldovich formula, the RHS of Eq (46) must be multiplied by the term

$$\frac{H\left[2c(T_s - T_i) - H - 2H_1 - \frac{2Q_1}{m}\right]}{\left[c(T_s - T_i) - H_1 - \frac{Q_1}{m}\right]^2} \quad . \tag{50}$$

These differences show that the Zeldovich equation is not rigorously valid in the limit of high activation energy. In particular, it yields in the standard case finite burning rates for all values of the ratio $c(T_s - T_i)/H$. Physically, it is clear that in this case all of these treatments must become invalid when $H \geq c(T_s - T_i)$, which corresponds to an adiabatic surface condition according to Eq (47). The general outcome is that conditions for which

$$H \gg c\,(T_s - T_i) - H_1 - \frac{Q_1}{m} \quad , \tag{51}$$

are excluded. Clearly, when the adiabatic condition is approached, the combustion wave will leave the surface and propagate into the interior of the solid, leaving behind essentially unsteady conditions between the wave and the surface. The physical way to avoid this to happen is to allow the surface temperature T_s to increase.

E. Overview of Theory

Particularly for double-base propellants, the dividing plane between the solid and gas phases is difficult to define. The process tends to be continuous, with the gas phase emerging clearly only towards the end of the fizz zone. The total amount of heat released by the end of the fizz zone is estimated to be about 500 cal/g[1]. However, the fraction H of this amount released in the solid phase is difficult to determine.* For this reason, it may be worth indicating that Eqs (46) and (47) can in fact be applied for any arbitrarily selected location of the solid-gas interface. It is only necessary that $(H + H_1)$ be the total amount of heat released per unit mass below the selected interface, and Q_1/m be the total amount of radiant energy absorbed per unit mass below this interface. At the end of the fizz zone, dT/dx becomes very nearly zero, except possibly at very high pressures. Therefore, for certain purposes, it may be desirable to select the "interface" x = 0 as the downstream-end of the fizz zone. Eq (47) then defines the corresponding "adiabatic" flame temperature T_s, and Eq (46) reduces to the classical Zeldovich–Frank-Kamenetski relationship for the flame speed[8]. The gas phase result of Appendix A can be viewed as a variation thereof.

With this last interpretation, it is easy to infer that the pressure influences the reaction rate; there is no impediment to assigning A a

---

**Reference 5 quotes a value of 350 cal/g for H and Reference 6 a value of 26 cal/g for H_1.*

pressure dependence (typically $A \propto P^{1.6}$ to obtain $m \propto P^{0.8}$) in order to obtain the pressure dependence of the burning rate. In the stricter interpretation, it is more difficult to allow A to depend on pressure, because external combustion pressure should influence reaction rates negligibly in the interior of the solid phase. Konev[6] offers a plausible argument, keeping A constant but allowing the surface temperature T_s to vary with pressure. It is done by maintaining the surface equilibrium for nitroglycerin in order to recover the pressure dependence of burning rate. The numerical values work out quite well, although the required heat of vaporization for nitroglycerin seems slightly high.

In so far as the effect of radiant flux at constant pressure is concerned, if the assumption of constant surface temperature is made[5,6], as justified in principle from the surface-equilibrium approach, then it becomes clear from Eq (46) that the radiation Q_1 is equivalent to an appropriate increase in initial propellant temperature, while the radiation Q_2 is totally ineffective. The agreement with experiment in Reference 6 supports this interpretation with $Q_2 = 0$.

Based on the present total study, this result appears to have general validity independent, for example, of the assumption of constant surface temperature. It is only necessary that some kinetic process, somewhere in either the solid or gas phase, be responsible for determining the burning rate. Then all radiation absorbed below the position where this kinetic process occurs is equivalent to a suitable increase in initial propellant temperature, while all radiation absorbed above this position is totally ineffective. The variation from being effective to being ineffective will take place continuously and monotonically.

IV. TEMPERATURE SENSITIVITY

A. Significance of the Parameter

The variation of burning rate with the initial temperature of the propellant at constant pressure is represented by the coefficient of temperature sensitivity. It gives the dependence on temperature, in

contrast with the pressure exponent that gives the dependence on pressure. However, the temperature sensitivity coefficient is amenable to formal treatment in the context of the theory of combustion thermal effects. Early studies on premixed gas flame theory produced the traditional Arrhenius form of the temperature sensitivity, and the more empirical forms which have been found useful in solid propellant combustion.[1]

When viewed as an experimental parameter, its customary role, the temperature coefficient offers the advantage of permitting calculations without the need of precise combustion models. Of course, the opposite applies, and the temperature sensitivity cannot be predicted with any degree of confidence unless accurate combustion models are known. If this is the case, the derivation is easily performed, as later shown with Eq (46). By definition, the coefficient of temperature sensitivity, denoted by $(\Pi_T)_p$, is

$$(\Pi_T)_p \equiv \left(\frac{\partial \ln(m/\rho)}{\partial T_i}\right)_p , \tag{52a}$$

$$\equiv \left(\frac{\partial \ln r}{\partial T_i}\right)_p , \tag{52b}$$

where subscript p means that the pressure is kept constant; r is the regression rate, i.e., the usual measurement of solid propellant burning rate. From Eq (52b), it is obtained explicitly that

$$\ln r = \ln r_o + \int_{T_{io}}^{T_i} (\Pi_T)_p \, dT , \tag{53}$$

and introducing Eq (18),

$$\ln r = \ln r_o + \int_{T_{io}}^{T_{io} + Q/r\rho c} (\Pi_T)_p \, dT . \tag{54}$$

Expressed differently, Eq (54) means that the effect of radiant flux can be obtained by measuring the burning rate at elevated initial temperatures. For high radiant fluxes, it may be necessary to calculate

iteratively, because the effective temperature depends on the burning rate r in the presence of external radiation. The new effective initial temperature is

$$T_i = T_{io} + \frac{Q}{r\rho c} \tag{55}$$

where T_{io} is a reference initial temperature, with no external radiation present. Sometimes the following approximation is made:

$$r = r_o \, e^{(\Pi_T)_p \; (T_i - T_{io})} , \tag{56}$$

where r is the burning rate at the higher initial temperature T_i, and r_o, the burning rate at the initial temperature T_{io}; $(\Pi_T)_p$ is the experimental coefficient for the temperature range T_{io} to T_i that satisfies Eq (56). This equation is consistent with Eqs (27) and (28) through the relation

$$(\Pi_T)_p = \frac{E}{2RT_f^2} \quad \frac{c}{c_p} , \tag{57}$$

which is the Arrhenius form of the temperature sensitivity coefficient. Changing Eq (56) into

$$r = r_o \exp \left[(\Pi_T)_p \frac{Q}{r\rho c} \right] , \tag{58}$$

gives a transcendental expression in r, although its inverse,

$$Q = \frac{r\rho c \ln(r/r_o)}{(\Pi_T)_p} , \tag{59}$$

is not transcendental in Q. An exact version of Eq (59), not dependent on the assumption of constant $(\Pi_T)_p$ is

$$Q = r\rho c \int_{r_o}^{r} \frac{dr}{(\Pi_T)_p r} . \tag{60}$$

When this simple approach cannot be taken, the only recourse is to delve into an analysis of the reaction zone.

B. Temperature and Pressure Dependence on $(\Pi_T)_p$

In a general sense, the temperature sensitivity of solid propellant combustion can exhibit dependences on both initial temperature and pressure, i.e., $\Pi_T = \Pi_T (T_i, P)$, as well as other variables. Double-base propellants display at least two distinct types of temperature sensitivity behavior, which lack definite theoretical explanation. The observation is that certain analogies exist between pressure and temperature dependences.

1. Linear Double-Base Propellants. The denomination "linear" is given here to that class of double-base propellants that, over an extended pressure range, exhibit a burning rate exponent n and temperature coefficient $(\Pi_T)_p$ which remain essentially independent of mean combustion pressure. This is the less complicated case and comprises many well known formulations. Propellants like JPN and N-4 belong to the linear class under typical rocket operating pressures and initial temperatures. It is often conventional to assign these propellants a constant "explosion" temperature T_e such that

$$r = \frac{f(P)}{T_e - T_i} = \frac{bP^n}{T_e - T_i} \quad , \tag{61}$$

where f(P) is a simple function of pressure, with constant coefficient b and exponent n. Despite the uncomplicated form of Eq (61), the agreement with experimental data for propellants burning in the linear regime is remarkably good. In this case,

$$(\Pi_T)_p = \frac{1}{T_e - T_i} \quad , \tag{62}$$

and no pressure dependence is involved. Figure 6 gives a plot of the calculated values for JPN and N-4 propellants as a function of initial temperature, in terms of Eq (62). It is seen that the temperature coefficient $(\Pi_T)_p$ increases less rapidly with initial temperature for the

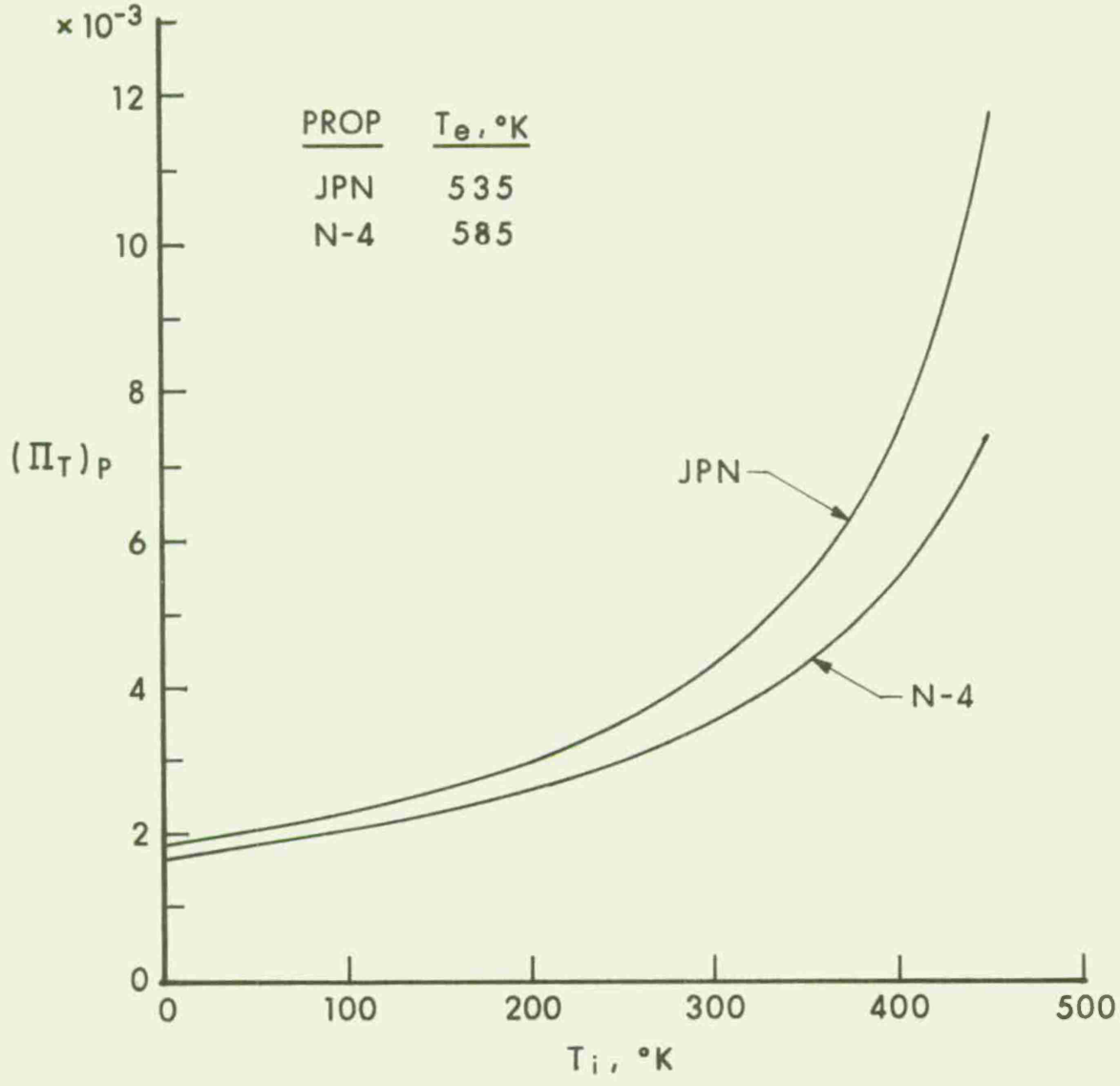

Figure 6. Calculated Temperature Coefficient for JPN and N-4 Double-Base Propellants.

larger T_e. In view of the above, Eq (61) can be rewritten as

$$r = (\Pi_T)_p \, f(P) \quad , \tag{63}$$

indicating that the burning rate, for the class of propellants under discussion, increases linearly with the temperature coefficient.

2. Mesa and Plateau Double-Base Propellants. These formulations are characterized by combustion regimes where both the pressure exponent and the temperature coefficient become strongly dependent on mean pressure, the latter retaining also a dependence on initial temperature of the type discussed before. This is the typical behavior of propellants like N-5 and X-14 which contain ingredients, lead and copper compounds, responsible for the mesa and plateau regimes. This burning behavior is of great interest but no present combustion models can fully interpret the complex pressure and temperature dependencies observed experimentally. Promising chemical schemes have been recently proposed by Kubota et al.[9], which give an insight into the difficulty of the analytical part of the problem. An analysis of the affected reaction zone might lead to expressions of the form

$$r = \frac{f(P)}{T_e(P) - T_i} \quad , \tag{64}$$

but solutions are, of course, unknown. Restricting the phenomenon to the experimental observation, the following behavior appears to be typical. For progressively higher pressures, the exponent n first increases and then diminishes rapidly as the mesa or plateau region is approached, later recovering as the region is surmounted at elevated pressures. Along with this variation of the pressure exponent, the temperature coefficient undergoes an almost parallel drastic reduction at the mesa or plateau region; in turn, the effect lessens quickly thereafter, as the burning rate passes this region and increases at higher pressures. This is the kind of trends reported by Kubota et al.[9] for the N-5 propellant; it is also evident for the X-14 propellant. Using experimental burning

rate data in conjunction with Eq (56), the calculated $(\Pi_T)_p$ values are shown in Figure 7 as a function of pressure. Apart from the theoretical interest of a possible interrelation between pressure exponent and temperature coefficient, the practical implications are important. Propellants having small temperature coefficients, whose dependence on initial temperature is also low, are generally believed to be the most suitable for application. However, the minimization of the temperature coefficient is bound to involve opposing requirements, and can only be properly resolved for each particular case.

C. Effect of Stabilizers

These compounds are widely used in double-base propellant formulations for the purpose of preventing undesirable chemical decomposition during storage. Konev[6] and others have advanced the idea that these substances could significantly contribute to the heat generated inside the solid phase as the propellant burns.

The detailed analysis of Section III and Appendix B was undertaken because of the potential importance of this effect, and its strong relevance toward mechanistic control of temperature sensitivity. The very comprehensive nature of the solution thus obtained, principally Eq (46), permits a confident prediction of the influence of stabilizers on the temperature sensitivity. Such a result is not possible without a solution like Eq (46). The overall indication is that larger temperature sensitivity $(\Pi_T)_p$ is to be expected as heat generation from the stabilizers increases. The theoretical result derived from Eq (46) is

$$(\Pi_T)_p = \frac{\gamma E_s}{2RT_s^2} + \frac{1-\gamma}{2(T_s-T_i) - \frac{H}{c} - \frac{2H_1}{c}} , \qquad (65)$$

where γ is a coefficient given by

$$\gamma = \frac{d}{dT_i} \left[\frac{\lambda T_s}{mc} \left(\frac{dT}{dx} \right)_s \right] . \qquad (66)$$

This coefficient is determined by the effect of the initial temperature

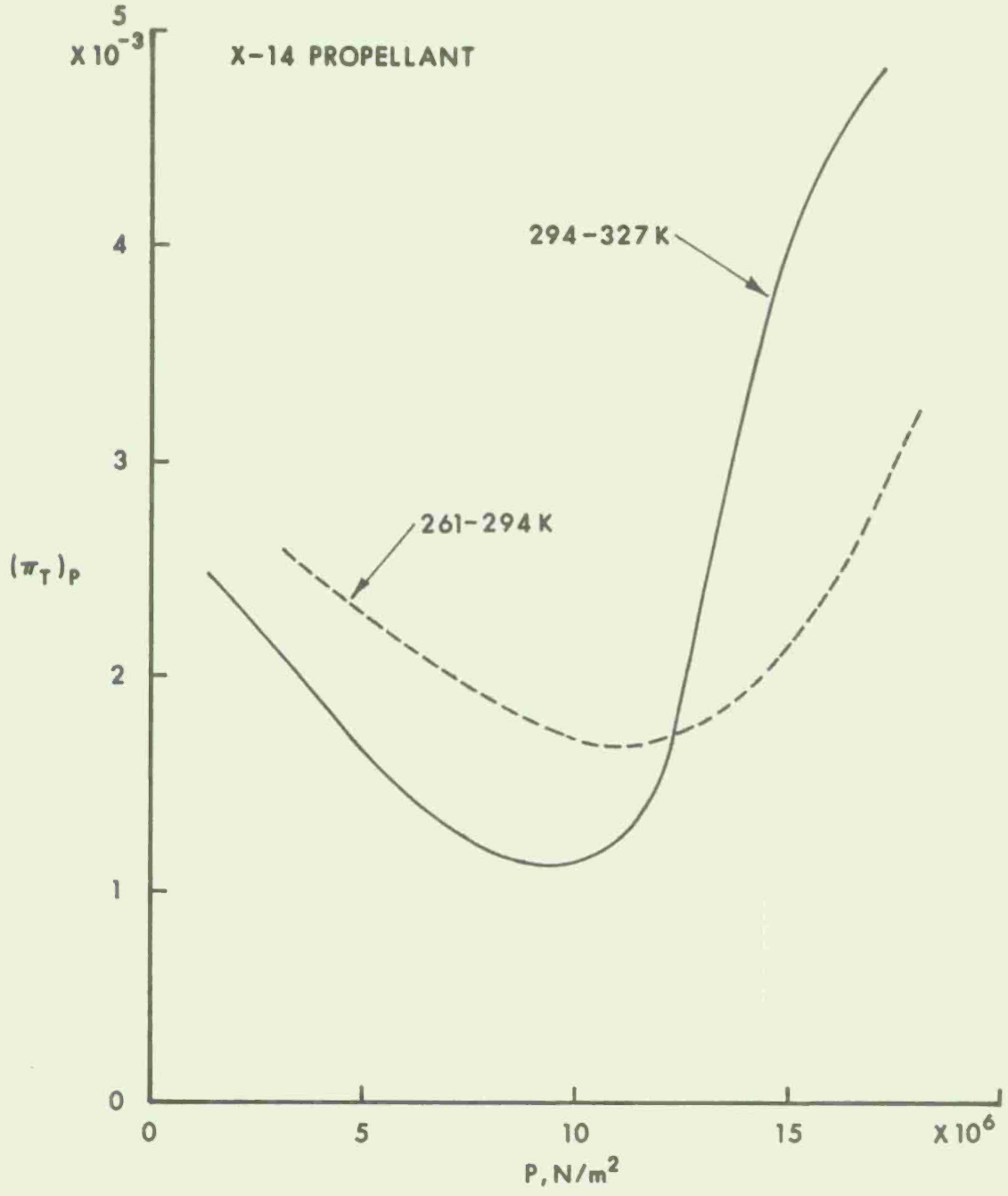

Figure 7. Observed Temperature Coefficient for X-14 Double-Base Propellant.

T_i on the surface temperature T_s. Numerically γ will vary between 0 and 1, reaching zero when T_s remains constant, although for most propellants is probably an intermediate value. As before, H is the heat generated in the solid phase by the main reaction, and H_l the heat generated by the reaction pertaining to the stabilizers. Since the surface temperature of burning double-base propellants is not that high, about 550°K, Eq (65) shows that the temperature coefficient can rapidly rise from its Arrhenius datum level even for modest increases of either of the two solid-phase heat generation terms, but primarily by increases from the stabilizers' term. The effect of H_l increments is twice as strong. Eq (65) equally shows the influence of the other variables of interest and suggests plausible ways to reduce the temperature sensitivity coefficient when the burning rate is under solid-phase reaction control.

In view of the practical significance of this result, experiments ought to be done to confirm the theoretical prediction. The experiment should be as follows: (1) Selection of a linear propellant (e.g., JPN) formulated with zero, low, medium and high concentrations of stabilizer; (2) determination of the heat generation terms from thermograms run at fast temperature-time conditions; (3) determination of $r(T_i,P)$ for each concentration of stabilizer, in order to calculate the temperature coefficients; and (4) comparison of results on the basis of stabilizer concentration for each combination of pressure and initial temperature. The measured heat generation terms might well not be the same as during combustion but should give an estimation of relative magnitude. Also, measurement of absorption coefficients would resolve the effect that stabilizer concentration might possibly have on this parameter.

V. COMPARISON WITH EXPERIMENT

A. Calculation Procedure

In view of the theoretical results, the best way to confront experimental evidence is on the basis that the radiant flux is equivalent to an increase in initial propellant temperature. The experimental verification of Eq (27) is not straightforward because, for a given propellant, there is no a priori knowledge on the exact value of the parameters K or K_s, especially for a wide pressure range. Therefore, the general form of the relationship that should be tested is as follows.

The experimentally-controllable variables influencing the burning rate r are the pressure, p, the initial temperature, T_i, and the radiant flux absorbed, Q. This dependence can be indicated by the functional relationship $r = r\ (P, T_i, Q)$. The equivalence of Q to an increase in initial temperature is expressed by the functional relationship

$$r\ (P, T_i, Q) = r\ (P, T_i + \frac{Q}{r\rho c}, 0). \tag{67}$$

Calculations are performed most conveniently by first selecting a value of pressure. For this pressure, and any other selected pressure thereafter, a tabulation of r as a function of T_i at $Q = 0$, and a tabulation of r as a function of Q at a fixed reference T_i, say $T_i = T_{io}$, must be available. In this manner, the effect of Q can be predicted from the $r(P, T_i)$ data and then compared with the effect observed experimentally at the reference temperature T_{io}. Thus, the objective is to find $r(P, T_{io}, Q)$. From the tabulation of r as a function of T_i, including T_{io}, r is known as a function of $T_i - T_{io}$, and then a value of Q is calculated for each entry from the equation

$$Q = r\rho c\ (T_i - T_{io})\ . \tag{68}$$

This enables the derived data of r as a function of Q, at each pressure, to be generated.

As explained before, the most suitable double-base propellants for this procedure are those exhibiting a linear burning regime at the pressures of interest, and whose temperature sensitivity coefficients are assigned a specific form, for example, the one given by Eq (62). Therefore, the relation of burning rate as a function of initial temperature can be used to calculate the effect of radiant flux on burning rate for propellants like JPN and N-4, for a wide range of pressures. Explicit predictions can be obtained for this class of propellants by noting that Eq (60) reduces in this case to

$$r = r_o + \frac{Qr_o}{\rho c f(p)} \quad , \tag{69}$$

or

$$\frac{r}{r_o} = 1 + \frac{Q}{r_o \rho c (T_e - T_{io})} \quad , \tag{70}$$

for fixed pressure conditions, and to

$$\frac{r}{r_o} = 1 + \frac{Q}{\rho c b P^n} \quad , \tag{71}$$

for variable pressure. These equations predict that the burning rate increases linearly with radiant flux, and that sizeable radiant fluxes are needed to increase the burning rate substantially, particularly at high pressures.

B. Experimental Measurements

Some test results have been obtained with the apparatus depicted in Figure 8. It consists of a source of radiant energy, a constant pressure combustion chamber, and optical elements to direct, divert and refocus the radiation beam on to the propellant surface. The chamber operates essentially as a strand-burner. Windows have been added to permit entrance of the radiation beam and for photography.

The radiant flux is measured at the position normally occupied by the propellant sample during initiation of burning. The measurement is

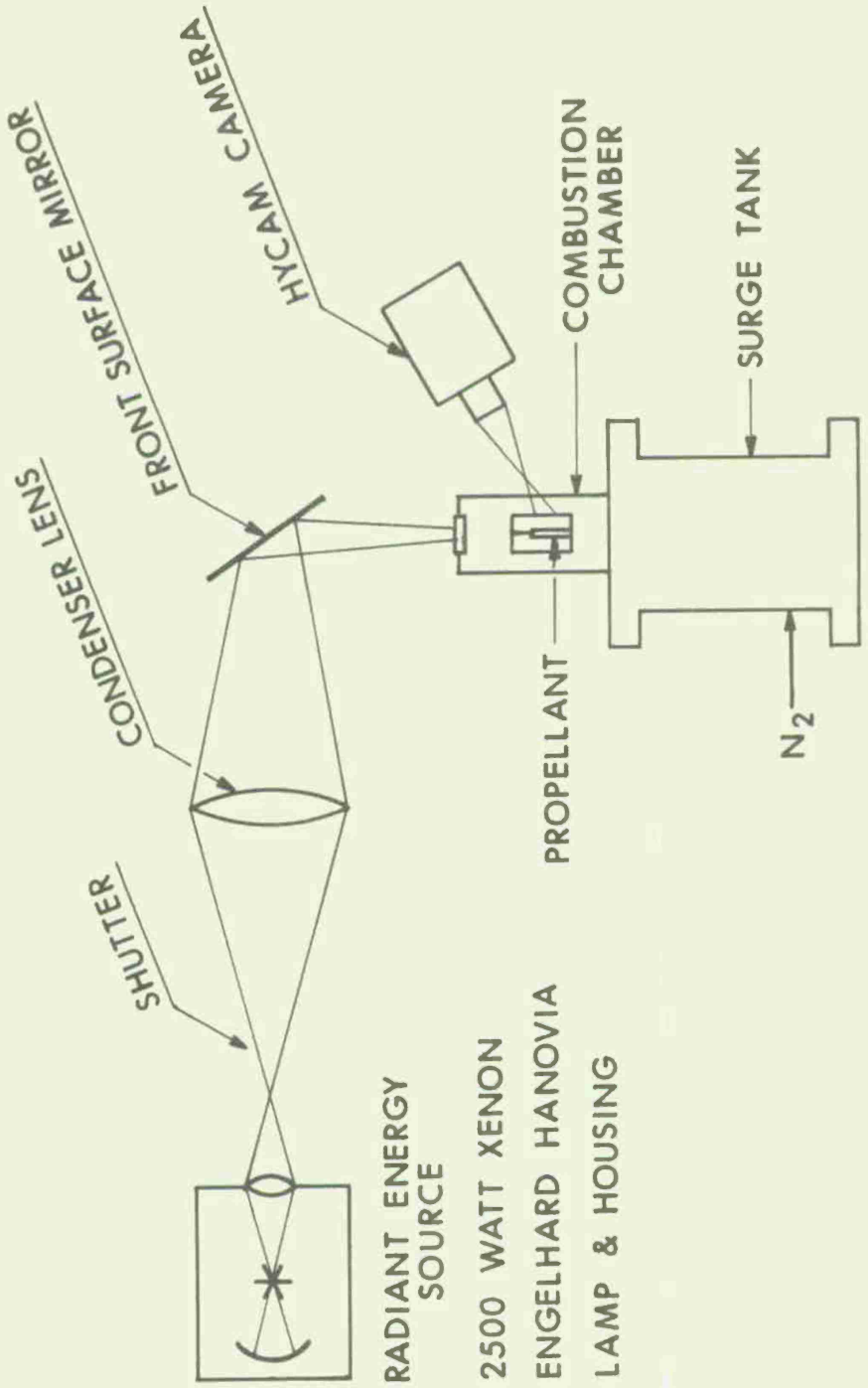

Figure 8. Experimental Apparatus.

made by using a water-cooled "Thermogage" continuous output calorimeter. No correction for gas absorption has been attempted and the nominal Q value so measured is carried into the calculations given later. The initial temperature of the propellant sample is monitored after pressurization of the chamber with a thermocouple placed adjacent to its surface. The propellant sample is a cylinder 1.2 cm in diameter and 2.4 cm in length, and otherwise prepared and mounted inside the chamber much in the same way as it is customary in strand burner operation. The burning of the propellant is recorded photographically by means of a high speed "Hycam" camera, outside illumination being provided by a mercury light. The burning rates with and without external radiation present are determined from timed readings of the regressing surface, taken by inspection of the photographic record. The radiant flux is not monitored during the course of the run; the diameter of the beam is initially about 3mm but some defocusing must occur as the surface regresses.

Many difficulties were encountered in performing the experiments, and the number of usable points eventually obtained is limited to a rather low Q value. Prevalent among the various difficulties is the requirement to control the initial temperature of the propellant accurately once a reference temperature has been selected. This is particularly critical when stimulating at low levels of radiation. It is clear that even small variations of initial temperature can have effects comparable to that of the external radiant flux, when only small stimulations are available. Such a condition is a direct consequence of Eq (68), which is shown in Figure 9. The technique for measuring the heat feedback from the gas flame alone was also intensively investigated at the beginning of the program. Here, the uncertain sensor response and light guide arrangement precluded the acquisition of reliable data.

C. Verification of Results

The original experimental plan included the testing of several propellants over a wide range of combustion pressures and stimulations

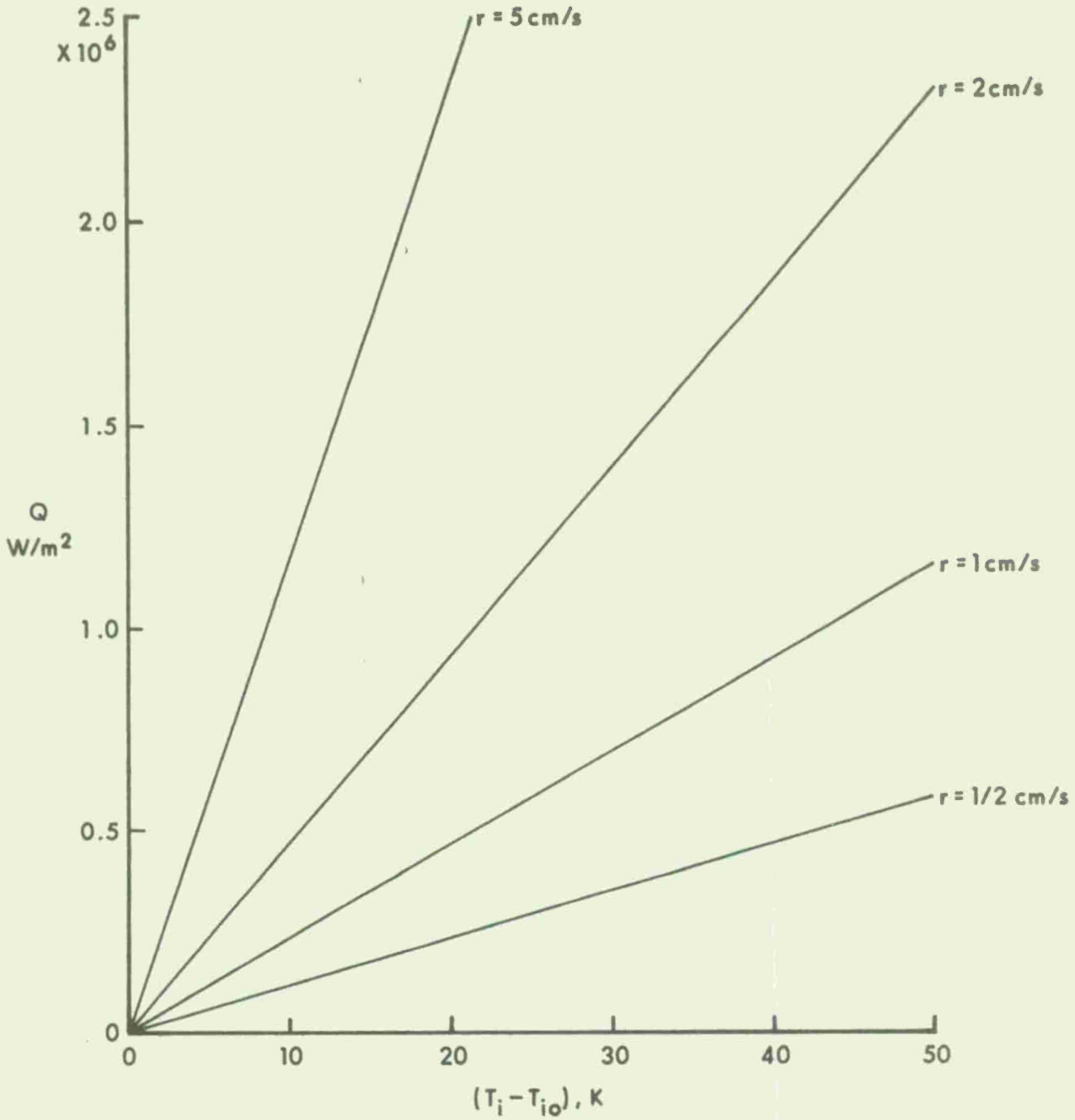

Figure 9. Equivalent Increase in Initial Propellant Temperature for Various Burning Rates.

of radiant flux. Only the JPN propellant could be tested, at a rather low flux level, but the data points extend to higher pressures than any previous results. These are listed in Table 1, which also contains the information on burning rate and propellant physical properties needed to calculate the predicted results. The burning rate determinations given in Table 1 are values derived over many readings of the film record. Additional data points were obtained at atmospheric pressure as a function of radiant flux stimulation. The results are presented in terms of the ratio r/r_o, where r_o is the normal burning rate and r the radiation-enhanced burning rate both at the same pressure.

The experimental results for the JPN propellant are shown in Figures 10 and 11, together with the predictions calculated from Eqs (70) and (71) respectively. Due to the intrinsic difficulty of distinguishing such small variations in burning rate, of the order of the precision of the experiment itself, the observed data scatter is not surprising. The data reported in Reference 6 were also analyzed and excellent agreement between observed and calculated results was found. On the basis of all available data, the view that, in so far as its effect on burning rate is concerned, radiant flux does nothing but effectively elevate the initial temperature of the propellant, appears to be supported quite well.

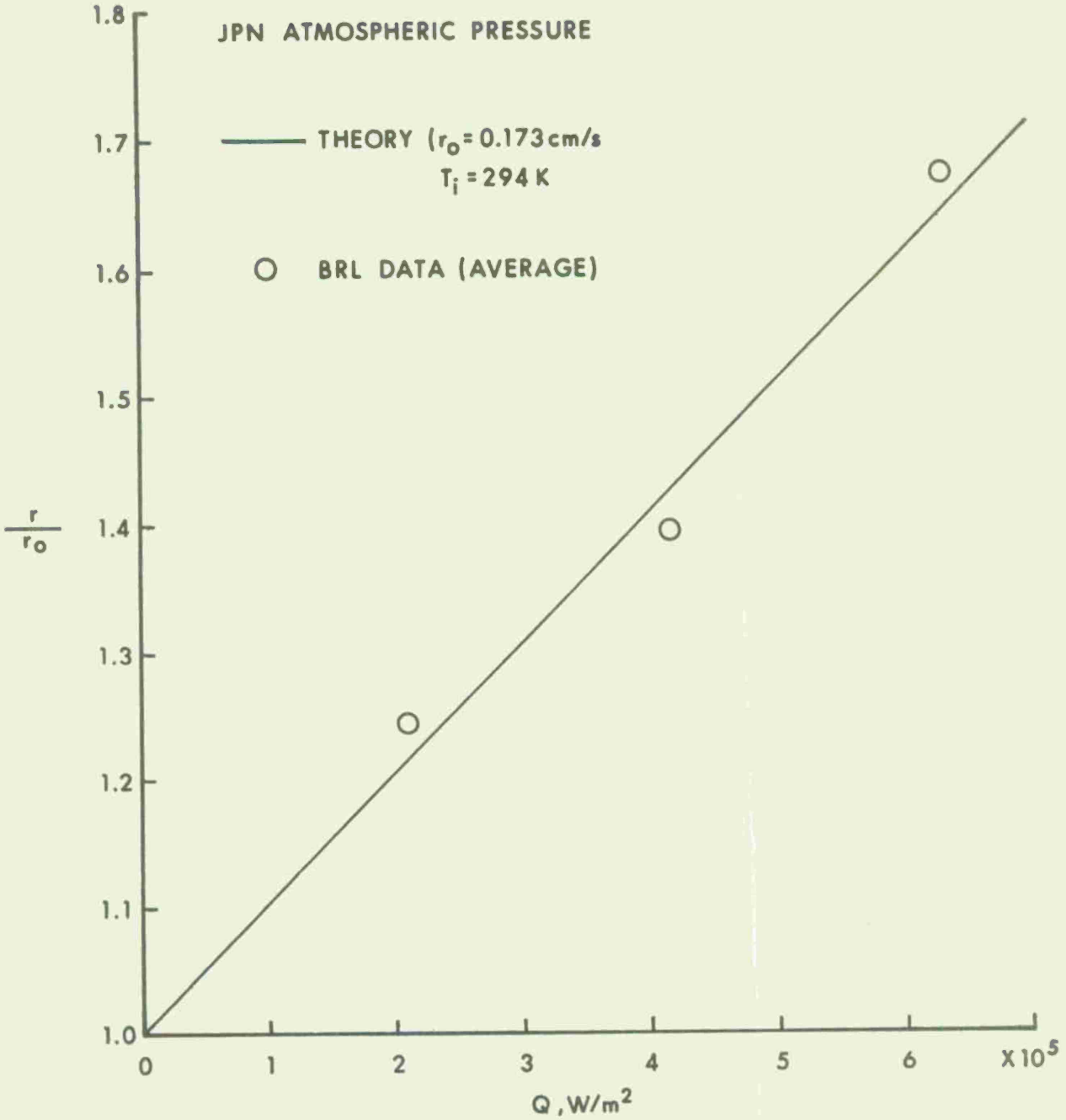

Figure 10. Observed and Calculated Burning Rate Augmentation for JPN Propellant at Atmospheric Pressure.

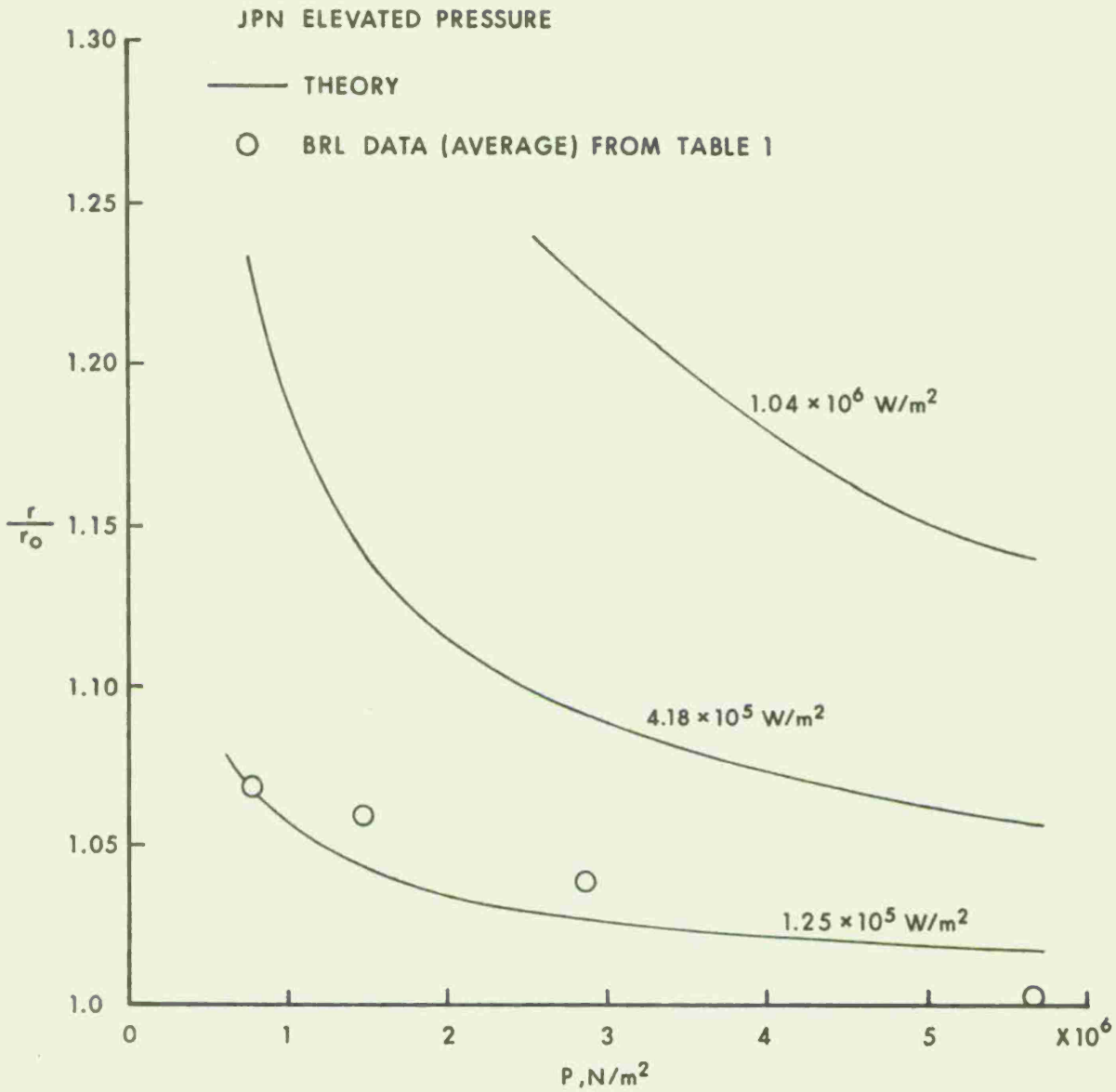

Figure 11. Observed and Calculated Burning Rate Augmentation for JPN Propellant at Elevated Pressures.

Table I.

Burning Rate Augmentation for JPN Propellant

Q = 0			Q ≈ 1.25×10^5 W/m^2		
0.79×10^6 N/m^2			0.79×10^6 N/m^2		
Test #	Init Temp. T_i, °K	Burn Rate r_o, cm/sec	Test #	Init. Temp	Burn Rate r, cm/sec
51	295	0.439	54	294	0.409
52	296	0.318	55	294	0.400
53	296	0.368	56	296	0.391
1.48×10^6 N/m^2			1.48×10^6 N/m^2		
40	294	0.465	49	294	0.587
41	293	0.505	50	295	0.485
			63	295	0.470
2.86×10^6 N/m^2			2.86×10^6 N/m^2		
37	295	0.864	44	294	0.932
42	292	0.724	47	293	0.813
67	295	0.818	48	295	0.787
			65	295	0.800
5.62×10^6 N/m^2			5.62×10^6 N/m^2		
58	296	1.24	60	295	1.22
59	296	1.30	61	295	1.26
			62	295	1.24

	Average Results		
Pressure P, N/m^2	r_o cm/sec	r cm/sec	r/r_o
0.79×10^6	0.375	0.400	1.067
1.48×10^6	0.485	0.514	1.059
2.86×10^6	0.802	0.833	1.038
5.62×10^6	1.27	1.24	0.98

Table I.

Burning Rate Augmentation for JPN Propellant (Cont'd)

Data for Prediction of Results

$$r = \frac{5.97 \times 10^{-5}}{535 - T_i} \; P^{0.70} \quad \text{m/sec}$$

(P, N/m^2; T_i, K)

$\rho = 1.6 \times 10^3$ Kg/m^3

$c = 1.46 \times 10^3$ J/Kg K

VI. DISCUSSION AND CONCLUSIONS

The analytical model developed here predicts realistically the effect of external thermal radiation on the burning rate of double-base propellants. Except for noted instances, the traditional hypothesis, that the effect can be treated as an increase in initial propellant temperature, has been found generally applicable. Therefore, the hypothesis is more properly referred to as an equivalence principle.

The experimental evidence shows satisfactory agreement between observed and predicted results, supporting the theoretical conclusion that the effect is calorific in nature and not directly dependent upon the chemistry of the combustion process. Owing to experimental difficulties, the amount of data collected in the BRL facility was small. The need for extensive new data, however, is not critical because of available results from other sources. Several other manifestations of thermal effects have been investigated, in particular the role of stabilizers in temperature sensitivity. Experiments to elucidate this important question are being planned.

The main conclusion is that the radiant energy absorbed by the propellant has the effect of raising the effective combustion temperature and therefore of enhancing the burning rate in a manner equivalent to an increase in initial temperature. For typical double-base propellants, the radiation effect will remain relatively constant with time; in rocket chambers the increase in burning rate over the strand-burner rate is normally less than 5%. On the contrary, transparent propellants will sustain a progressive effect on burning rate; if large amounts of radiant energy are absorbed deep in the interior of the solid, other effects like cracking and fissuring can appear. Such effects are not included here.

The conclusions are also far reaching in regard to the effect of stabilizers. The rise in temperature by heat conduction within the solid initiates the decomposition of nitroglycerin and nitrocellulose according to traditional notions. These are exothermic processes liberating an

amount of heat represented in the theory by the term H. A second type of reaction within the solid that can contribute equally substantial amounts of heat is the one postulated between the nitrate ester decomposition products and the stabilizers, represented in the theory by the term H_1. The function of these compounds is well known and has been mentioned before. The fact is that self heating must increase with stabilizer concentration.

The problem of temperature sensitivity is basically part of the general theory of thermal effects. The concern here has been to emphasize the role of this parameter in the theory and to show that it can be predicted with confidence only to the extent that the combustion model used is realistic. The scope of the analysis has lead to a generalization of the Zeldovich[7] formula and temperature sensitivity prediction in which the effect of stabilizer concentration, among other parameters, is clearly indicated. Increasing the concentration of a stabilizer that reacts at low temperature increases the temperature sensitivity through the term H_1; however, twice as large of an increase in the heat release H of the main solid reaction is needed to produce an equivalent augmentation. Therefore, stabilizer modifications are predicted to have a large effect.

Future analytical studies will consider the influence of radiant flux when such a stimulus is applied in the oscillatory mode.

ACKNOWLEDGMENT

The authors wish to thank Dr. I. W. May and Mr. R. A. Wires for their information on experimental absorption coefficients.

REFERENCES

1. Huggett, Clayton, Bartley, C.E., and Mills, Mark M., "Solid Propellant Rockets", Princeton University Press, Princeton, New Jersey, (1960).

2. Linan, A., and Williams, F. A., "Radiant Ignition of a Reactive Solid with in-depth Absorption", Combustion and Flame, 18, 85 (1972).

3. Lengelle, G., "Thermal Degradation Kinetics and Surface Pyrolysis of Vinyl Polymers", AIAA Journal, 8, 1989 (1970).

4. Coates, R. L., and Kwak, S., "The Effect of External Radiation on the Burning Rate of Solid Propellants", J. Spacecraft and Rockets, 9, 742 (1972).

5. Konev, E.V., and Khlevnoi, S. S., "Burning of a Powder in the Presence of Luminous Radiation", Combustion, Explosion and Shock Waves, 2 (4), 21 (1966). (Faraday Press Translation).

6. Kovalskii, A. A., Konev, E. V., and Krasilnikov, B. V., "Combustion of Nitroglycerine Powder", Combustion, Explosion and Shock Waves, 4 (4), 336 (1968). (Faraday Press Translation).

7. Zeldovich, Ya. B., "On the Theory of Combustion of Powders and Explosives", Zh. Eksperim. i Teor. Fiz., 12, 498 (1942).

8. Williams, Forman A., Combustion Theory", Chapter 5, Addison-Wesley Publishing Co., Inc., Reading, Massachusetts, (1965).

9. Kubota, N., Ohlemiller, T.J., Caveny, L. H., and Summerfield, M., "The Mechanism of Super Rate Burning of Catalyzed Double Base Propellants", Aerospace and Mechanical Sciences Report No. 1087, Princeton University, Princeton, New Jersey, March 1973.

APPENDIX A
ANALYSIS OF GAS-PHASE REACTION ZONE

Using the present notation, the gas-phase flame exists in the region $x>0$. The quasisteady conservation equations for energy and for reactant mass fraction are

$$mc_p \frac{dT}{dx} = \lambda_g \frac{d^2T}{dx^2} + H_g BYP^\nu e^{-E/RT} \quad , \tag{A1}$$

and

$$m \frac{dY}{dx} = \rho_g D \frac{d^2Y}{dx^2} - BYP^\nu e^{-E/RT} \quad , \tag{A2}$$

respectively, where m is the mass burning rate, c_p, the heat capacity at constant pressure, λ_g, the thermal conductivity, ρ_g, the density, H_g, the heat released per unit mass of reactant consumed, B, the preexponential factor in the Arrhenius rate expression, Y, the reactant mass fraction, ν, the order of reaction, E, the activation energy and D, the diffusion coefficient. The boundary conditions for Eqs (A1) and (A2) are

$$T = T_s \quad \text{at} \quad x = 0 \tag{A3a}$$

$$m(1 - Y) = -\rho_g D \frac{dY}{dx} \quad \text{at } x = 0 \tag{A3b}$$

$$mL = \lambda_g \frac{dT}{dx} \quad \text{at} \quad x = 0 \ , \tag{A3c}$$

and

$$Y = 0 \quad \text{at } x = \infty \ , \tag{A4}$$

where L in Eq (A3c) is the sum of the heat of gasification and the heat conducted into the interior of the solid, both per unit mass of reactant consumed. A number of simplifying assumptions are introduced; for example, the thermal conductivity and the diffusivity $\rho_g D$ have been assumed constant. The reaction has been assumed to be first order with respect to the reactant, although an arbitrary order ν has been permitted insofar as the pressure dependence is concerned. It is later introduced

that $\rho_g D = \lambda_g / c_p \equiv \alpha$ is a constant, justified since the Lewis number is assumed to be unity[A1]. The dependent variables, as well as the pressure, P, the mass rate, m, the surface temperature, T_s and the heat, L, are all considered to be functions of time; the heat transfer to the solid enters through L.

Dividing Eq (A1) by H_g and adding the result to Eq (A2) gives

$$m \frac{d(Y + \Theta)}{dx} = \alpha \frac{d^2(Y + \Theta)}{dx^2} \tag{A5}$$

where $\Theta \equiv c_p T / H_g$ is a nondimensional gas temperature. The only solution to Eq (A5) remaining bounded at infinity is a constant. Evaluating the constant by using Eq (A4) gives

$$Y = \Theta_f - \Theta \ , \tag{A6}$$

where the time dependent flame temperature T_f is nondimensionalized as $\Theta_f = c_p T_f / H_g$. Substitution of Eq (A6) into Eq (A3b) reveals that at $x = 0$,

$$m(1 + \Theta_s - \Theta_f) = \alpha \frac{d\Theta}{dx} \ , \tag{A7}$$

where Θ_s applies to the surface. Eqs (A3c) and (A7) lead to the solution

$$\Theta_f = 1 + \Theta_s - z \tag{A8}$$

where $z \equiv L / H_g$ is the nondimensional parameter accounting for the heat flux into the solid. Substitution of Eq (A6) into Eq (A1) produces the equation

$$m \frac{d\Theta}{dx} = \alpha \frac{d^2\Theta}{dx^2} + B P^{\nu} (\Theta_f - \Theta) e^{-E'/\Theta} \ , \tag{A9}$$

where $E' \equiv E c_p / R H_g$ is a nondimensional activation energy. The boundary conditions for Eq (A9) are

$$\Theta = \Theta_s \quad \text{at} \quad x = 0 \ , \tag{A10a}$$

from Eq (A3c),

$$\alpha \frac{d\theta}{dx} = mz \text{ at } x = 0 , \tag{A10b}$$

and

$$\theta = \theta_f \text{ at } x = \infty . \tag{A11}$$

From the analysis of Bush and Fendell[A2], it is known that in the limit of large activation energy, there is a convective-diffusive zone occupying a position θ which is not very close to θ_f. See Figure A1 for definitions. In the convective-diffusive zone, the last term in Eq (A9) is negligible, and the general solution is

$$\theta = a + b\, e^{mx/\alpha} , \tag{A12}$$

where a and b are constants of integration. The boundary conditions of Eqs (A10a) and (A10b) may be used to evaluate the constants of integration, giving

$$\theta = \theta_s + z\,(e^{mx/\alpha} - 1) . \tag{A13}$$

In this solution, it is seen by using Eq (A8) that $\theta = \theta_f$ at $x = x_f$, where

$$x_f = \left(\frac{\alpha}{m}\right) \ln\left(\frac{1}{z}\right) , \tag{A14}$$

is to lowest order ($E' \to \infty$) the distance between the solid surface and the gas-phase reaction zone. Differentiating Eq (A13) and using Eq (A14) gives

$$\frac{d\theta}{dx} = \frac{m}{\alpha} \text{ at } x = x_f . \tag{A15}$$

For large activation energy, there exists in lowest order a reactive-diffusive zone about the position x_f. In this zone, the first term in Eq (A9) is negligible. The appropriate stretched spatial variable is

$$\eta \equiv \frac{\beta m(x - x_f)}{\alpha} , \tag{A16}$$

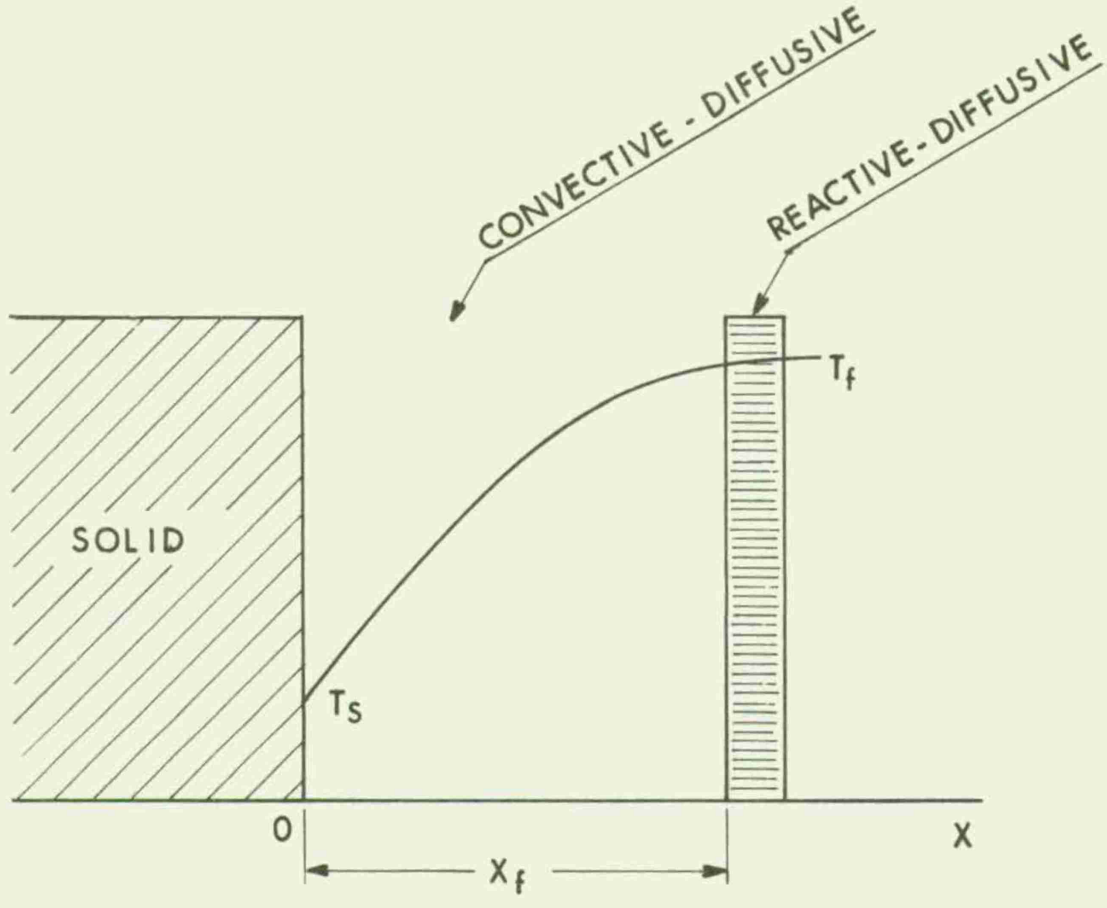

Figure A1. Gas-Phase Reaction Zones.

where the large expansion parameter is

$$\beta \equiv \frac{E'}{\theta_f^2} = \frac{EH_g}{c_p R T_f^2} \quad , \tag{A17}$$

and Eq (A9) reduces in lowest order to

$$\frac{d^2y}{d\eta^2} = \Lambda y e^{-y} \quad , \tag{A18}$$

where

$$y \equiv \beta (\theta_f - \theta) \quad , \tag{A19}$$

is the stretched nondimensional temperature, and

$$\Lambda \equiv \left(\frac{\alpha B P^\nu}{m^2 \beta^2}\right) e^{-E'/\theta_f} \quad . \tag{A20}$$

The boundary conditions for Eq (18), derived by matching from Eq (A15) and from the condition of Eq (A11), are

$$y \to 0 \quad \text{as} \quad \eta \to \infty \quad , \tag{A21}$$

and

$$\frac{dy}{d\eta} \to -1 \quad \text{as} \quad \eta \to -\infty \quad . \tag{A22}$$

Eqs (A18), (A21) and (A22) define the classical problem for the flame-speed eigenvalue for a premixed laminar flame. The solution is $\Lambda = 1/2$ [A2,A3]. Therefore the result from Eq (A20) is

$$m = \left[\frac{2\alpha R^2 T_f^4 c_p^2 B P^\nu}{E^2 H_g^2}\right]^{1/2} e^{-E/2RT_f} \quad . \tag{A23}$$

Although a factor T_f^2 emerges from the square root, it can be eliminated by assigning suitable temperature dependences to α or B; in any event, for large activation energy the effect of that factor is small compared with the effect of the exponential term. Hence, Eq (A23) can be written as

$$m = C P^{\nu/2} e^{-E/2RT_f} \quad , \tag{A24}$$

where the coefficient C is independent of time. Eq (A24) is the burning rate prediction for the gas-phase flame.

REFERENCES

A1. Williams, Forman A., "Combustion Theory", Chapter 5, Addison-Wesley Publishing Co., Inc., Reading, Massachusetts, (1965).

A2. Bush, W. B., and Fendell, F. E., "Asymptotic Analysis of Laminar Flame Propagation for General Lewis Numbers", Combustion Science and Technology, 1, 421 (1970).

A3. Williams, F. A., "Theory of Combustion in Laminar Flows", in "Anual Reviews of Fluid Mechanics", (Edited by M. van Dyke and W. G. Vincenti), Vol. 3, p 171 (1971), Anual Reviews Inc., Palo Alto, California.

APPENDIX B
ANALYSIS OF SOLID-PHASE REACTION ZONE

Asymptotic considerations show that a reactive-diffusive zone exists at the surface of the solid phase when the activation energy is large. The definitions are the same as in Figures 4 and 5. In this reactive-diffusive zone, the proper spatial variable is defined by

$$\eta \equiv - \frac{\beta m c x}{\lambda} , \tag{B1}$$

where in turn, the nondimensional activation energy β is defined by

$$\beta \equiv \frac{E_s}{RT_s} . \tag{B2}$$

In this zone, the relevant temperature variable ζ is defined by

$$\zeta \equiv \frac{\beta(T_s - T)}{T_s} , \tag{B3}$$

and the following nondimensional groups are introduced for transformation of the differential equations:

$$h \equiv \frac{H}{cT_s} , \tag{B4}$$

$$a \equiv \frac{\mu\lambda RT_s}{mcE_s} , \tag{B5}$$

and

$$b \equiv \frac{\mu\lambda RQ_2}{m^2 c^2 E_s} . \tag{B6}$$

Expressing the nondimensional burning rate in the form

$$\Psi = m \left[\frac{E_s c}{RT_s \lambda \rho A e^{-E_s/RT_s}} \right]^{1/2} , \tag{B7}$$

Eq (35),

$$m \frac{dY}{dx} = -\rho A e^{-E_s/RT} = -w ,$$

becomes

$$\frac{dY}{d\eta} = \frac{1}{\psi^2} e^{-\frac{\zeta}{(1-\zeta/\beta)}} \quad ; \tag{B8}$$

and Eq (36),

$$mc \frac{dT}{dx} = \lambda \frac{d^2T}{dx^2} + Hw + Q\mu e^{\mu x} \quad ,$$

becomes

$$\frac{d^2\zeta}{d\eta^2} + \frac{1}{\beta} \frac{d\zeta}{d\eta} = \frac{h}{\psi^2} e^{-\frac{\zeta}{(1-\zeta/\beta)}} + b e^{-a\eta} \quad . \tag{B9}$$

The boundary conditions for Eqs (B8) and (B9) are

$$Y = 0 \quad \text{at} \quad \eta = 0 \quad , \tag{B10a}$$

and

$$\zeta = 0 \quad \text{at} \quad \eta = 0 \quad . \tag{B10b}$$

To lowest order in the small parameter β^{-1}, matching conditions are found to be

$$Y \to 1 \text{ as } \eta \to \infty \quad , \tag{B11a}$$

and

$$\frac{d\zeta}{d\eta} \to C \quad \text{as} \quad \eta \to \infty \quad . \tag{B11b}$$

Here the value of the constant C is derived from Eq (45) with the result that

$$C \equiv \frac{\left(T_s - T_i - \frac{H_1}{c} - \frac{Q_1}{mc} \right)}{T_s} \quad . \tag{B12}$$

Since solutions are sought only to lowest order in the small parameter β^{-1}, Eq (8B) simplifies to

$$\frac{dY}{d\eta} = \frac{1}{\psi^2} e^{-\zeta} \quad , \tag{B13}$$

and Eq (B9) simplifies to

$$\frac{d^2\zeta}{d\eta^2} = \frac{h}{\psi^2} e^{-\zeta} + b e^{-a\eta} \quad . \tag{B14}$$

The integral of Eq (B13), subject to the previously specified boundary conditions Eqs (B10a,b) and Eqs (B11a,b), provides an expression for the burning rate,

$$\psi^2 = \int_0^\infty e^{-\zeta} \, d\eta \quad . \tag{B15}$$

The remaining problem is to solve Eq (B14), subject to the previously specified boundary conditions of Eqs (B10b) and (B11b). With the absorptive term, $b e^{-a\eta}$, included in full, Eq (B14) cannot be solved analytically. Therefore, only the limiting case $a \to \infty$ will be considered, as explained in Section III. This produces a thin surface layer in which all the radiation is absorbed, while ζ changes very little. Within this layer, the appropriate spatial variable is

$$\varepsilon = a\eta \ , \tag{B16}$$

and the appropriate temperature variable is

$$\phi = \frac{a^2\zeta}{b} \quad . \tag{B17}$$

Thus Eq (B14) becomes

$$\frac{d^2\phi}{d\varepsilon^2} = \frac{h}{\psi^2 b} e^{-b\phi/a^2} + e^{-\varepsilon} \quad . \tag{B18}$$

As $a \to \infty$, the last term of Eq (B18) tends towards a constant, and the solution becomes

$$\phi = \left(\frac{h}{2\psi^2 b}\right) \varepsilon^2 - (1 - e^{-\varepsilon}) + \textit{constant}\ \varepsilon. \tag{B19}$$

The constant is to be determined by matching with the reactive-diffusive zone. It is seen from Eq (B18) that, to lowest order in a^{-1}, the structure of the reactive-diffusive zone is unaffected by the presence of the absorption layer.

For the reactive-diffusive zone, Eq (B14) is

$$\frac{d^2\zeta}{d\eta^2} = \frac{h}{\psi^2}\, e^{-\zeta} \quad , \tag{B20}$$

with lowest order boundary conditions specified again by Eqs (B10b) and (B11b). The first integral of Eq (B20) is

$$\frac{1}{2}\left(\frac{d\zeta}{d\eta}\right)^2 = \frac{h}{\psi^2}\int_{\infty}^{\zeta} e^{-\zeta}\, d\zeta + \frac{1}{2}C^2 = \frac{1}{2}C^2 - \frac{h}{\psi^2}e^{-\zeta} \quad . \tag{B21}$$

The integral of Eq (B21) is

$$\eta = \int_0^{\zeta} \frac{d\zeta}{\left(C^2 - \frac{2h}{\psi^2}e^{-\zeta}\right)^{1/2}} \quad . \tag{B22}$$

From Eq (B15) it follows that

$$\psi^2 = \int_0^{\infty} e^{-\zeta}\left(\frac{d\eta}{d\zeta}\right) d\zeta$$

$$= \int_0^{\infty} \frac{e^{-\zeta}\, d\zeta}{\left(C^2 - \frac{2h}{\psi^2}e^{-\zeta}\right)^{1/2}}$$

$$= \frac{C\psi^2}{h}\left[1 - \left(1 - \frac{2h}{C^2\psi^2}\right)^{1/2}\right], \tag{B23}$$

whence

$$\psi^2 = \left(C - \frac{h}{2}\right)^{-1} \quad . \tag{B24}$$

This is the burning rate expression, which by means of Eqs (B7) and (B12), can be written dimensionally as

$$m^2 = \frac{RT_s^2\lambda\rho A\, e^{-E_s/RT_s}}{E_s\left[c(T_s - T_i) - \frac{H}{2} - H_l - \frac{Q_l}{m}\right]} \quad . \tag{B25}$$

This analysis shows that the surface temperature gradient is determined by the solution, because the derivative of Eq (B22) implies that at $x = 0$

$$\left(\frac{d\zeta}{d\eta}\right)_s = C - h \ , \tag{B26}$$

so that Eq (47) follows. The significance of all these theoretical developments is presented in Sections III and IV.

DISTRIBUTION LIST

No. of Copies	Organization
12	Commander Defense Documentation Center ATTN: DDC-TCA Cameron Station Alexandria, Virginia 22314
1	Director Institute for Defense Analysis ATTN: Dr. H. Wolfhard 400 Army-Navy Drive Arlington, Virginia 22202
2	Commander U.S. Army Materiel Command ATTN: AMCDMA Mr. N. Klein Mr. J. Bender 5001 Eisenhower Avenue Alexandria, Virginia 22333
1	Commander U.S. Army Materiel Command ATTN: AMCRD, BG H.A. Griffith 5001 Eisenhower Avenue Alexandria, Virginia 22333
1	Commander U.S. Army Materiel Command ATTN: AMCRD-T 5001 Eisenhower Avenue Alexandria, Virginia 22333
1	Commander U.S. Army Materiel Command ATTN: AMCRD-MT 5001 Eisenhower Avenue Alexandria, Virginia 22333
1	Commander U.S. Army Aviation Systems Command ATTN: AMSAV-E 12th and Spruce Streets St. Louis, Missouri 63166
1	Director U.S. Army Air Mobility Research and Development Laboratory Ames Research Center Moffett Field, California 94035
1	Commander U.S. Army Electronics Command ATTN: AMSEL-RD Fort Monmouth, New Jersey 07703
1	Commander U.S. Army Missile Command ATTN: AMSMI-R Redstone Arsenal, Alabama 35809
1	Commander U.S. Army Tank Automotive Command ATTN: AMSTA-RHFL Warren, Michigan 48090
2	Commander U.S. Army Mobility Equipment Research & Development Center ATTN: Tech Docu Cen, Bldg. 315 AMSME-RZT Fort Belvoir, Virginia 22060
1	Commander U.S. Army Armament Command Rock Island, Illinois 61202
4	Commander U.S. Army Frankford Arsenal ATTN: SARFA-PDC, Dr. Lannon SARFA-MDS, Mr. Dickey SARFA-MDS, Mr. Kucsan SARFA-MDP, Mr. Mitchel Philadelphia, Pennsylvania 19137

DISTRIBUTION LIST

No. of Copies	Organization
2	Commander U.S. Army Picatinny Arsenal ATTN: SARPA-VG, Dr. J.Picard Mr. Lenchitz Dover, New Jersey 07801
1	Commander U.S. Army White Sands Missile Range ATTN: STEWS-VT White Sands, New Mexico 88002
1	Commander U.S. Army Harry Diamond Laboratories ATTN: AMXDO-TI 2800 Powder Mill Road Adelphi, Maryland 20783
1	Commander U.S. Army Materials and Mechanics Research Center ATTN: AMXMR-ATL Watertown, Massachusetts 02172
1	Commander U.S. Army Natick Laboratories ATTN: AMXRE, Dr. D. Sieling Natick, Massachusetts 01762
1	Commander U.S. Army Research Office (Durham) ATTN: Tech Lib Box CM, Duke Station Durham, North Carolina 27706
5	Commander U.S. Naval Air Systems Command ATTN: AIR-5366 AIR-5367 AIR-604 (3 cys) Washington, DC 20360
3	Commander U.S. Naval Ordnance Systems Command ATTN: ORD-0632 ORD-035 ORD-5524 Washington, DC 20360
1	Chief of Naval Research ATTN: ONR-429 Department of the Navy Washington, DC 20360
1	Commander U.S. Naval Missile Center ATTN: Code 5632 Point Mugu, California 93041
3	Commander U.S. Naval Weapons Center ATTN: Code 608 Mr. J. Crump Dr. R. Derr Code 753, Tech Lib China Lake, California 93555
1	Commander U.S. Naval Ordnance Laboratory ATTN: Code 730 Silver Spring, Maryland 20910
1	Director U.S. Naval Research Laboratory ATTN: Code 6180 Washington, DC 20390
1	Commander U.S. Naval Weapons Laboratory ATTN: Tech Lib Dahlgren, Virginia 22338
1	Superintendent U.S. Naval Postgraduate School ATTN: Tech Lib Monterey, California 93940

DISTRIBUTION LIST

No. of Copies	Organization
2	Commander U.S. Naval Ordnance Station ATTN: Dr. A. Roberts Tech Lib Indian Head, Maryland 20640
1	AFSC (DOL) Andrews AFB Washington, DC 20331
1	AFOSR (SREP) 1400 Wilson Boulevard Arlington, Virginia 22209
2	AFRPL (RPMCP Dr. R. Weiss; Dr. R. Schoner) Edwards AFB California 93523
2	Headquarters National Aeronautics and Space Administration ATTN: RPS RP Washington, DC 20546
1	Director NASA Scientific and Technical Information Facility ATTN: CRT P. O. Box 33 College Park, Maryland 20740
1	Director National Aeronautics and Space Administration George C. Marshall Space Flight Center ATTN: Tech Lib Huntsville, Alabama 35812
1	Director Jet Propulsion Laboratory ATTN: Tech Lib 4800 Oak Grove Drive Pasadena, California 91103
1	Director John F. Kennedy Space Center National Aeronautics and Space Administration ATTN: Tech Lib Kennedy Space Center Florida 32899
1	Director National Aeronautics and Space Administration Langley Research Center ATTN: MS-185, Tech Lib Langley Station Hampton, Virginia 23365
1	Director National Aeronautics and Space Administration ATTN: MS-603, Tech Lib MS-86, Dr.L.Povinelli 21000 Brookpark Road Lewis Research Center Cleveland, Ohio 44135
1	Director National Aeronautics and Space Administration Manned Spacecraft Center ATTN: Tech Lib Houston, Texas 77058
1	Aeroject Solid Propulsion Co ATTN: Dr. P. Micheli Sacramento, California 95813
1	ARO Incorporated ATTN: Mr. N. Dougherty Arnold AFS Tennessee 37389
1	Atlantic Research Corporation ATTN: Tech Lib Shirley Highway at Edsall Road Alexandria, Virginia 22314

DISTRIBUTION LIST

No. of Copies	Organization
1	General Electric Company Flight Propulsion Division ATTN: Tech Lib Cincinnati, Ohio 45215
2	Hercules Incorporated Allegany Ballistic Labs ATTN: Dr. R. Young Tech Lib Cumberland, Maryland 21501
1	Hercules Incorporated Bacchus Division ATTN: Dr. M. Beckstead Magna, Utah 84044
1	Lockheed Palo Alto Research Laboratories ATTN: Tech Info Center 3251 Hanover Street Palo Alto, California 94304
1	Lockheed Propulsion Company ATTN: Dr. N. Cohen P. O. Box 111 Redlands, California 92373
1	McDonnell Douglas Corporation Missile and Space Systems Division ATTN: Tech Lib Santa Monica, California 90406
1	The Martin-Marietta Corporation Denver Division ATTN: Res Lib P. O. Box 179 Denver, Colorado 80201
2	North American Rockwell Corp Rocketdyne Division ATTN: Dr. C. Oberg Tech Lib 6633 Canoga Avenue Canoga Park, California 91304
2	North American Rockwell Corp Rocketdyne Division ATTN: Mr. W. Haymes Tech Lib McGregor, Texas 76657
1	Thiokol Chemical Corporation Elkton Division ATTN: E. Sutton Elkton, Maryland 21921
3	Thiokol Chemical Corporation Huntsville Division ATTN: Dr. D. Flanigan Dr. R. Glick Tech Lib Huntsville, Alabama 35807
2	Thiokol Chemical Corporation Wasatch Division ATTN: Dr. John Peterson Tech Lib P. O. Box 524 Brigham City, Utah 84302
1	TRW Systems Group ATTN: Mr. H. Korman One Space Park Redondo Beach, California 90278
1	United Aircraft Corporation Pratt and Whitney Division ATTN: Tech Lib P. O. Box 2691 West Palm Beach, Florida 33402
2	United Technology Center ATTN: Dr. R. Brown Tech Lib P. O. Box 358 Sunnyvale, California 94088

DISTRIBUTION LIST

No. of Copies	Organization
1	Battelle Memorial Institute ATTN: Tech Lib 505 King Avenue Columbus, Ohio 43201
1	Brigham Young University Dept of Chemical Engineering ATTN: Prof. R. Coates Provo, Utah 84601
2	California Institute of Technology ATTN: Prof. F. Culick Tech Lib 1201 East California Boulevard Pasadena, California 91102
1	Case Western Reserve University Division of Aerospace Sciences ATTN: Prof. J. Tien Cleveland, Ohio 44135
2	Calspan Corporation ATTN: E. B. Fisher A. P. Trippe P. O. Box 235 Buffalo, New York 14221
2	Georgia Institute of Technology School of Aerospace Engineering ATTN: Prof. B. Zinn Prof. E. Price Atlanta, Georgia 30333
1	IIT Research Institute ATTN: Prof. T. Torda 10 West 35th Street Chicago, Illinois 60616
1	Director Applied Physics Laboratory The Johns Hopkins University 8621 Georgia Avenue Silver Spring, Maryland 20910
2	Director Chemical Propulsion Information Agency The Johns Hopkins University ATTN: Mr. T. Christian Tech Lib 8621 Georgia Avenue Silver Spring, Maryland 20910
1	Massachusetts Institute of Technology Dept of Mechanical Engineering ATTN: Prof. T. Toong Cambridge, Massachusetts 02139
2	Pennsylvania State University Dept of Mechanical Engineering ATTN: Prof. G. Faeth Prof. K. Kuo University Park, Pennsylvania 16802
4	Princeton University Department of Aerospace and Mechanical Sciences ATTN: Prof. M. Summerfield Prof. I. Glassman Dr. L. Cavney Tech Lib James Forrestal Campus Princeton, New Jersey 08540
2	Purdue University School of Mechanical Engineering ATTN: Prof. J. Osborn Prof. S.N.B. Murthy Lafayette, Indiana 47907
1	Rutgers-State University Dept of Mechanical and Aerospace Engineering ATTN: Prof. S. Temkin University Heights Campus New Brunswick, New Jersey 08903

DISTRIBUTION LIST

No. of Copies	Organization
1	Stanford Research Institute Propulsion Sciences Division ATTN: Tech Lib 333 Ravenswood Avenue Menlo Park, California 94024
1	Stevens Institute of Technology Davidson Laboratory ATTN: Prof. R. McAlevy III Hoboken, New Jersey 07030
2	University of California Dept of Aerospace Engineering ATTN: Prof. S. Penner Prof. F. Williams La Jolla, California 92037
1	University of California Dept of Chemistry ATTN: Prof. E. Peterson Berkeley, California 94704
1	University of Denver Denver Research Institute ATTN: Tech Lib P. O. Box 10127 Denver, Colorado 80210
2	University of Illinois Dept of Aeronautical Engineering ATTN: Prof. H. Krier Prof. R. Strehlow Urbana, Illinois 61803
1	University of Minnesota Dept of Mechanical Engineering ATTN: Prof. E. Fletcher Minneapolis, Minnesota 55455
2	University of Utah Dept of Chemical Engineering ATTN: Prof. A. Baer Prof. G. Flando Salt Lake City, Utah 84112
	Aberdeen Proving Ground
	Marine Corps Ln Ofc Dir, USAMSAA